

2



TECHNICAL REPORT
NATICK/TR-93/011

AD-A260 126

AD _____



OPTICAL ANALYSIS OF LENSLET ARRAYS

by

John P. Kurmer
Wolf P. Altman
John S. Laudo
Daniel R. Grieser
Jane F. O'Loughlin
Van E. Wood

BATTELLE
505 King Avenue
Columbus, Ohio 43201-02693

Edward M. Healy*

December 1992

Final Report

December 1988 -- October 1991

93-00646



DTIC
ELECTE
JAN 2 1993
S E D

APPROVED FOR PUBLIC RELEASE; DISTRIBUTION UNLIMITED

Prepared for

UNITED STATES ARMY NATICK
RESEARCH, DEVELOPMENT AND ENGINEERING CENTER
NATICK, MASSACHUSETTS 01760-5000

*SOLDIER SCIENCE DIRECTORATE

08 1 17 0 12

DISCLAIMERS

The findings contained in this report are not to be construed as an official Department of the Army position unless so designated by other authorized documents.

Citation of trade names in this report does not constitute an official endorsement or approval of the use of such items.

DESTRUCTION NOTICE

For Classified Documents:

Follow the procedures in DoD 5200.22-M, Industrial Security Manual, Section II-19 or DoD 5200.1-R, Information Security Program Regulation, Chapter IX.

For Unclassified/Limited Distribution Documents:

Destroy by any method that prevents disclosure of contents or reconstruction of the document.

REPORT DOCUMENTATION PAGE

Form Approved
OMB No. 0704-0186

Public reporting burden for this collection of information is estimated to average 1 hour per response, including the time for reviewing instructions, searching existing data sources, gathering and maintaining the data needed, and completing and reviewing the collection of information. Send comments regarding this burden estimate or any other aspect of this collection of information, including suggestions for reducing this burden, to Washington Headquarters Services, Directorate for Information Operations and Reports, 1215 Jefferson Davis Highway, Suite 1204, Arlington, VA 22202-4302 and to the Office of Management and Budget, Paperwork Reduction Project (0704-0186), Washington, DC 20503.

1. AGENCY USE ONLY (Leave blank)		2. REPORT DATE December 1992	3. REPORT TYPE AND DATES COVERED Final Contract Report; 88/12/22-91/10/31	
4. TITLE AND SUBTITLE OPTICAL ANALYSIS OF LENSLET ARRAYS			5. FUNDING NUMBERS DAAR60-89-C-0010	
6. AUTHOR(S) Kurmer, John P.; Altman, Wolf P.; Laudo, John S.; Grieser, Daniel R.; O'Loughlin, Jane F.; Wood, Van E.; Healy, Edward M.*				
7. PERFORMING ORGANIZATION NAME(S) AND ADDRESS(ES) BATTELLE 505 King Avenue Columbus, OH 43201-2693			8. PERFORMING ORGANIZATION REPORT NUMBER	
9. SPONSORING, MONITORING AGENCY NAME(S) AND ADDRESS(ES) U. S. Army Natick Research, Development & Engineering Center Kansas Street Natick, MA 01760-5020			10. SPONSORING MONITORING AGENCY REPORT NUMBER NATICK/TR-93/011	
11. SUPPLEMENTARY NOTES *The professional affiliation of Edward M. Healy is U.S. Army Natick RD&E Center.				
12a. DISTRIBUTION AVAILABILITY STATEMENT Approved for public release, distribution unlimited			12b. DISTRIBUTION CODE	
13. ABSTRACT (Maximum 200 words) Designs were developed of arrays of small-diameter (2-4mm) unity-power telescopes to be used with nonlinear optical materials in the protection of the eyes against tunable lasers. A ray-tracing program (Super-Oslo™) was used to design lenslets and predict the performance of four-lens telescopes (quads). Lens types adjudged most promising were aspheres, curved graded-index (GRIN), and kinoform (diffractive) combined with spherical. Variables included lenslet diameter, f-number, quad length, and optical gain. Packing configurations utilized square, round and hexagonal quads. Properties evaluated included resolution, field of view, aberrations, tolerances, and overall usefulness as components in compact, lightweight goggle elements. Commercial arrays of lenslets were evaluated and found unacceptable. Bi-aspheric lenslets were designed and injection-molded. Lenses from the first supplier were unacceptable, but high-quality lenses were obtained from a second source. An array of 76 lenslet elements, constructed for evaluation of visual characteristics, showed fair optical quality.				
14. SUBJECT TERMS EYE PROTECTION, LASER, LENSLET OPTICAL ANALYSIS ARRAYS			15. NUMBER OF PAGES 85	
			16. PRICE CODE	
17. SECURITY CLASSIFICATION OF REPORT UNCLASSIFIED			18. SECURITY CLASSIFICATION OF THIS PAGE UNCLASSIFIED	
			19. SECURITY CLASSIFICATION OF ABSTRACT UNCLASSIFIED	
20. LIMITATION OF ABSTRACT				

TABLE OF CONTENTS

	<u>Page</u>
LIST OF ILLUSTRATIONS	iv
PREFACE	vii
1.0 EXECUTIVE SUMMARY	1
2.0 INTRODUCTION	3
2.1 Program Objectives	3
2.2 Eye Protection Requirements	4
2.3 Summary Of Technical Approach	6
2.4 Summary Results Of Phase I	12
2.5 Summary Results Of Phase II	13
2.6 Summary Results Of Phase III	14
2.7 Summary Results Of Phase IV	14
3.0 PHASE I EFFORTS	16
3.1 Lenslet Types Evaluated	16
3.2 Experimental Verification of Model	22
3.3 Lenslet Array Packing Configurations	23
3.4 Ghost Images on the Retina of the Eye	26
4.0 PHASE II EFFORTS	28
4.1 Off-Axis Performance Characteristics of the Lenslet Elements	28
4.2 Optical Engineering Guidelines	32
4.3 Preliminary Nonlinear Optical Phenomena Assessment	33
5.0 PHASE III EFFORTS	39
5.1 Lenslet Eyepiece, Goggle Design and Fabrication	39
5.2 Conical Quad Design	45
5.3 Baseline Lenslet Design Performance Characteristics - PROTO90Q	46
5.4 Initiation of Subcontract to Mold Custom Lenslet Design	54
6.0 PHASE IV EFFORTS	58
6.1 Experimental Evaluation of Custom Molded Lenslets	58
6.2 Estimated Manufacturing Costs	68
7.0 CONCLUSIONS	74
8.0 RECOMMENDATIONS	76
9.0 REFERENCES	78

LIST OF ILLUSTRATIONS

<u>Figure</u>	<u>Page</u>	
1	Maximum Permissible Exposure (MPE) for Direct Ocular Intrabeam Viewing of Single Laser Pulses	5
2	Reduction of MPE for Repetitively Pulsed Lasers	5
3	The Eye and Spectral Characteristics	7
4	Biological Effects on the Eye from Laser Radiation Exposure	8
5	Schematic Representation of the Device Showing How an Upright Image Would be Transferred	9
6	Helmholtz Model of the Eye	11
7	Computer Schematic of the Eye Model	11
8	Modulation Transfer Function (MTF), Resolution, and Visual Acuity of the Human Eye	12
9	Commercially Available Spherical Lens, Aeroflex	18
10	Modified Aeroflex Lens with Aspherical Surface	18
11	Commercially Available Flat Surface GRIN Lens, Melles Griot	19
12	Commercially Available Spherical Surface GRIN Lens, Melles Griot	19
13	Modified Melles Griot Spherical Lens with Conjectured Curvature	19
14	Commercially Available Spherical Ball Lens, Melles Griot	20
15	Binary Optical Element	20
16	Kinform with Asphere Design	21
17	Refractive Achromat Design	21
18	Test Station for Optically Evaluating Lenslet Arrays	22
19	Naked Eye Resolution	24
20	Single Pair Aeroflex Lenses Resolution	24
21	Array Geometry Spot Diagrams	25
22	Ghost Images	27
23	Sketch of First-Order Ghosts Visible in Paired-Aeroflex Experiments	27
24	Optical Performance of the Quad Asphere and the Quad Kinoform with Sphere as a Function of Field Angle	29
25	Optical Performance of the Quad Kinoform with Sphere and the Kinoform with Asphere as a Function of Field Angle	29
26	Optical Performance of the Quad Kinoform with Asphere and the Aspheric GRIN as a Function of Field Angle	30
27	Optical Field Angle Performance Summary of Four Quad Lenslet Designs	30
28	Optical Performance of the Aspheric Achromat as a Function of Field Angle	31
29	Comparison of Visual Acuity for Human Eyes and the Aspheric Design as a Function of Field Angle	32
30	Design Parameter Space	33
31	Self-Focusing — Self-Defocusing	35
32	Various Proposed Optical Limiting and Switching Concepts	38
33	Light Rays Incident on the Pupil Focus on the Retina	40
34	Radial Placement of Lenslets in the Goggles Results in a Wide Field of View	40
35	Goggle Design Centered on Eye's Center of Rotation	41
36	Image Transfer of an Object 10 m Away from the Observer	41

LIST OF ILLUSTRATIONS
(continued)

Figure	Page
37 Front View of Lenslet Eyepiece	43
38 Humphrey Field Analyzer Visual Performance Tests	44
39 Laser Eye Protection Goggles	44
40 Conical Lenslet Quad Design	45
41 Optical System Layout PROTO90Q	47
42 Comparison of Spot Diagrams: (a) Without and (b) With Lenslet Array	48
43 Visual Spot Size for Conical Quad Aspheres	49
44 Wavefront Error for PROTO90Q Quad	50
45 Percent Light Transmission of Lenslet Quad	51
46 Performance Comparison of Various Lenslet Systems	52
47 Gain Degradation as Function of Incident Angle for First Lenslet Element - PROTO90Q	53
48 Engineering Drawing of Lenslet Quad Produced by Plastec, Inc.	56
49 Engineering Drawing of Lenslet Element Tooling Produced by Plastec, Inc.	57
50a Representative Sample of the Optical Quality of the Fabricated Lens 1 Design Received from Plastec, Inc.	59
50b Representative Sample of the Optical Quality of the Fabricated Lens 2 Design Received from Plastec, Inc.	59
50c Representative Sample of the Optical Quality of the Fabricated Lens 3 Design Received from Plastec, Inc.	60
50d Representative Sample of the Optical Quality of the Fabricated Lens 4 Design Received from Plastec, Inc.	60
51a Spot Size of Lens 1 as Seen by CCD Camera 200 μ m in Front of Best Focus	61
51b Spot Size of Lens 1 as Seen by CCD Camera at Best Focus	61
51c Spot Size of Lens 1 as Seen by CCD Camera 200 μ m Behind Best Focus	61
52a 3-Bar Test Chart as Seen Directly by Camera	63
52b 3-Bar Test Chart as Seen by Two Precision Optics, Inc. Lenslets	63
53a 3-Bar Test Chart as Viewed Through Four Precision Optics, Inc. Lenslets	65
53b 3-Bar Test Chart as Viewed Through Four OPKOR, Inc. Lenslets	65
53c 3-Bar Test Chart as Viewed Through Two Custom-Molded Plastec, Inc. Lenslets	65
54 Focal Region Contour Maps for Various Lenslets Available	66
55 3-D Profile and Contour Map of Custom Molded Lens from OPKOR, Inc.	67
56 Photograph of Video Display High Contrast	68
57 Computer Simulation Using PROTO90Q FOV Resolution	69
58 Photograph of Video Display Through OPKOR Quad	69
59 Proposed Future Efforts	77

Table

1 Summary of Lenslet Types Evaluated	17
2 Nonrecurring and Production Costs of Quads	70
3 Nonrecurring and Production Costs of Goggles	72

PREFACE

This is Battelle's final report to U.S. Army Natick Research, Development and Engineering Center on the research program entitled "Optical Analysis of Lenslet Arrays". The work was funded under Natick contract DAAK60-89-C-0010 and was performed in four six-month phases between December 22, 1988 and October 31, 1991. This report summarizes in Sections 2.4 to 2.7 the progress under each of the phases.

The citation of trade names in this report does not constitute official endorsement or approval of the use of an item.

Accession For	
NTIS CRA&I	<input checked="" type="checkbox"/>
DTIC TAB	<input type="checkbox"/>
Unannounced	<input type="checkbox"/>
Justification	
By	
Distribution /	
Availability Codes	
Dist	Avail and/or Special
A-1	

OPTICAL ANALYSIS OF LENSLET ARRAYS

1.0 EXECUTIVE SUMMARY

The objective of this program was to assess and demonstrate the optical performance of arrays of small lenses that, when used in conjunction with nonlinear optical (NLO) materials and incorporated into goggles or visors, could be used to protect the eyes against frequency-agile laser threats. This effort included evaluating various lenslet element types and configurations to determine their performance characteristics with respect to resolution, field of view (FOV), aberrations, tolerances, and overall usefulness as a compact, lightweight, goggle element.

During the initial phases of this program, commercially available lenslet arrays were used to verify experimentally the mathematical models developed and to obtain a first-order estimate of the anticipated visual performance of the lenslet array concept. During the latter phases of this program, custom bi-aspheric lenslets were fabricated, using an injection molding process, to increase the overall optical performance of the lenslet array goggle device. Through the course of this program, it became evident that custom-molded lenslets would be required to achieve the required level of optical performance. Commercially available lenslets do not provide sufficient optical quality within the packing length required.

Under Phase I, an evaluation of the on-axis performance of various lenslet elements including spherical, aspherical, gradient index (GRIN), and binary optical elements was performed; additionally, the experimental verification of a spherical lenslet array was initiated. In Phase II, the evaluation of lenslet elements continued and was extended to include more complex lenslet elements along with modeling the off-axis optical performance. Phase II also included preliminary assessment of a hemispherical lenslet array to better typify use as a goggle or helmet device. First-order estimates of the requirements on the nonlinear optical (NLO) materials were also initiated. In Phase III, effort concentrated on developing a bi-aspheric lenslet design because it was the most promising theoretically and could be fabricated using present day technology. A subcontract was initiated to Plastec, Inc., to fabricate the custom lenslets required. Finally, in Phase IV, it was found that Plastec, Inc., was unable to meet the design tolerances for the lenslet elements and a second subcontract was initiated to OPKOR, Inc. OPKOR, Inc. was able to meet the design requirements and a 76-element lenslet array was fabricated. This array indicated, but did not thoroughly demonstrate, the feasibility of making a lenslet array of sufficient optical quality to be useful in an eye protection device utilizing nonlinear optical material. Preliminary manufacturing costs for making a lenslet array in production were also investigated.

This program is seen by the authors as the first of a series of efforts to develop a fully functional frequency-agile eye protection device. Many questions concerning the viability of using a lenslet array as an eye protection device have been answered; however, many more remain.

Section 2 describes the program objectives, eye protection requirements, and a summary of the technical approach used in this effort. This is followed by a brief summary of the major accomplishments obtained in each of the four phases.

Section 3, 4, 5, and 6 describe, in some detail, the methodology used and the results obtained for each of the four phases. Section 7 provides the conclusions for this effort, while Section 8 contains a series of recommended additional efforts that are believed necessary and that must be initiated in a timely manner in order to develop a fully functional eye protection device. Finally, Section 9 provides a list of references used in this work.

2.0 INTRODUCTION

2.1 Program Objectives

The objective of this program was to conduct an optical analysis of lenslet arrays to determine their applicability in laser eye protection and to address some of the fabrication issues. Theoretical modeling was used to develop optical designs that had optical performance characteristics superior to commercially available spherical lenslet arrays. In addition, preliminary lenslet fabrication was initiated.

The objectives of Phases I and II addressed issues related to:

- Assessing the feasibility of being able to see through a lenslet array
- Assessing the feasibility of having high-acuity vision with a large field of view when looking through the array
- Being able to correct for chromatic distortion introduced by simple lenslets
- Developing a goggle device that could be small and lightweight enough to be used by Army personnel
- Developing a goggle device such that it would not impede the mission significantly.

Under Phases III and IV, these analytical results were extended to include initial lenslet array design and fabrication. The objectives of Phases III and IV addressed issues related to:

- Designing of an initial lenslet array and assembly technique
- Fabricating lenslet elements, spacers, and a suitable holder
- Demonstrating initial feasibility of the lenslet concept
- Demonstrating good on-axis performance with limited field of view but not chromatically corrected.

The ultimate goal of this program is to develop a device that could protect the eyes from pulsed, frequency-agile, visible lasers. In addition to meeting the laser threat requirements, the protection device must also be light weight and easily incorporated into a face mask or helmet. It must allow a large enough FOV in order not to hinder the sight of the person wearing the unit. The unit must be comfortable to wear and not require any special training or other operating procedures. In an ideal case, it would be nothing more than an entirely passive (requiring no power supply) clear face visor or windshield. The current program, for which this is the final report, is a first attempt at addressing these difficult ultimate goals. Several additional funded efforts will be required to refine and extend the work performed under this contract.

2.2 Eye Protection Requirements

The laser eye protection problem is extremely broad in its potential scope, encompassing continuous wave (CW) and pulsed sources and potential wavelengths from the ultraviolet (UV) to the infrared (IR) regions of the spectrum. The eye protection device must not degrade visual performance as long as there is no threat (an off-state transmission greater than 75% is desired); however, as soon as a threat is present, the shutter must be capable of switching to an effective high optical density (on-state OD of 4.0 or greater) to block the incident radiation. This switch must be done sufficiently fast so that the eye is not damaged (required switching time should be less than 1 ns). When the threat is no longer present, the shutter device must quickly reduce its effective optical density allowing unobstructed observation. Protection is required throughout the 400 to 700 nm spectral band; out-of-band threats can be handled by low- and high-pass fixed filters, which are relatively immune to destruction by optical means. The requirement of the shutter device to respond effectively throughout the visible region requires that a nonresonant NLO phenomenon, or at least a phenomenon with a very large response bandwidth, be utilized. Finally, the device must be durable enough to remain functional during and after exposure to high-power pulses and CW threats. It may be possible eventually to combine the fast responding nonlinear optical approach with a slower responding electro-optical approach that would tune a notch filter to the desired wavelength to allow the mission to be performed while under an extended CW attack.

The American National Standard for the safe use of lasers (ANSI-Z 136.1-1986) sets a limit on the maximum permissible exposure of visible laser radiation incident on the eye at $0.5 \mu\text{J}/\text{cm}^2$ for single shot pulses of duration between 1 ns - 18 μs , as shown in Figure 1. A multiplicative derating factor must be used as indicated in Figure 2 for repetitive pulses incident on the eye. The limit is 1 mW/cm^2 for extended exposure up to 10 s to CW radiation.

• Intrabeam Viewing (7 mm aperture)

400 - 700 nm 1 ns - 18 μ s 0.5 μ J/cm²

18 μ s - 10 s 1.8 t^{3/4} mJ/cm²

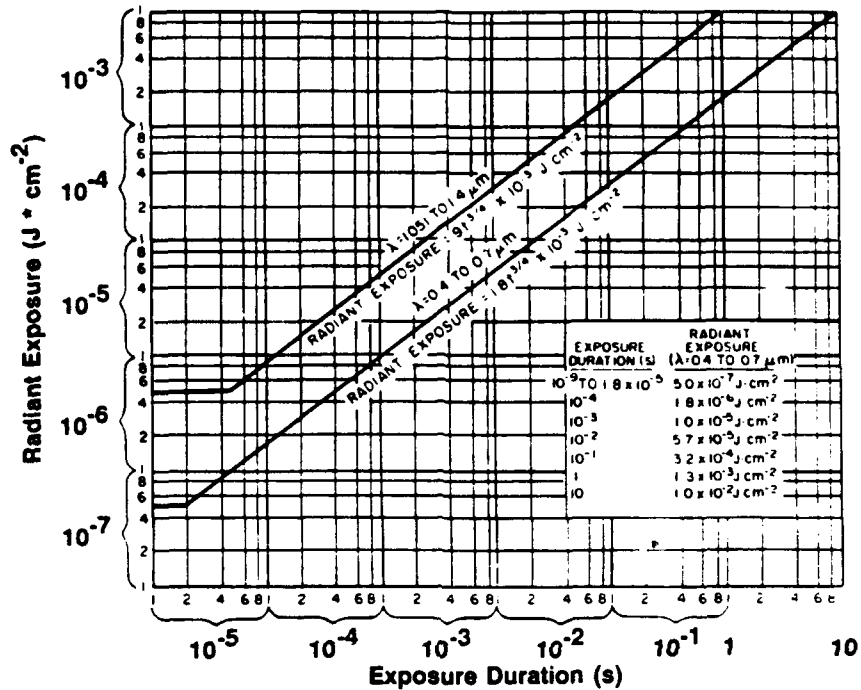


Figure 1 Maximum Permissible Exposure (MPE) for Direct Ocular Intrabeam Viewing of Single Laser Pulses (ANSI-Z 136.1-1986)

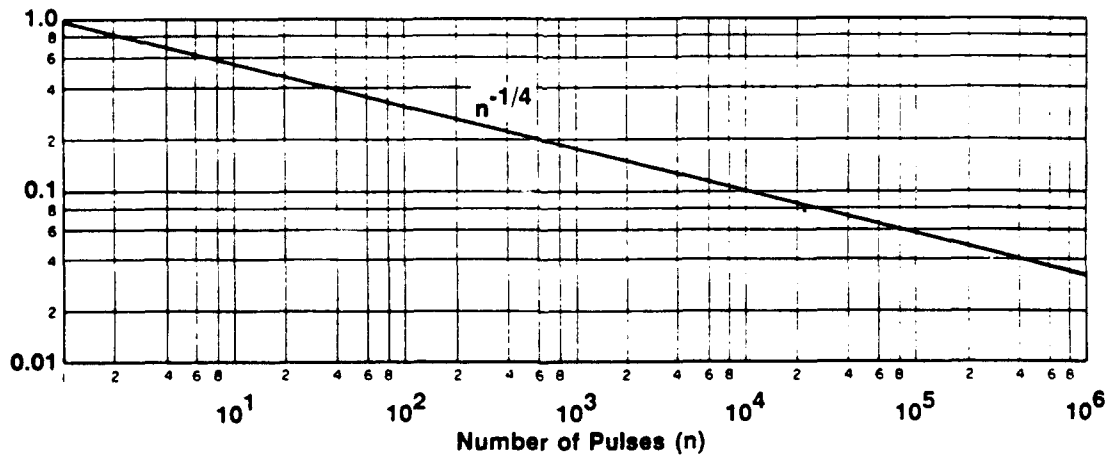


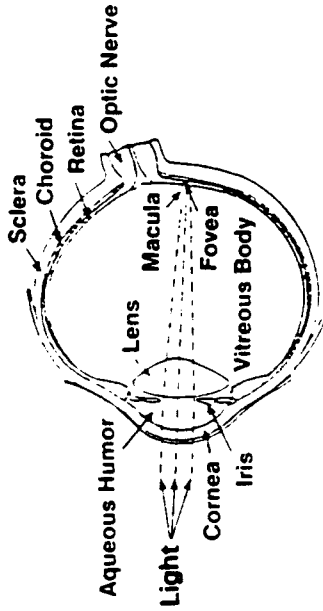
Figure 2 Reduction of MPE for Repetitively Pulsed Lasers

Transmittance through the ocular media and the absorption in the retina and the choroid of the eye are shown in Figure 3. It can be seen that the ocular media is greater than 95% transmitting in the visible region, while the retina and choroid show significant absorption. The biological effects of various wavelengths of light incident on the eye are shown in Figure 4.

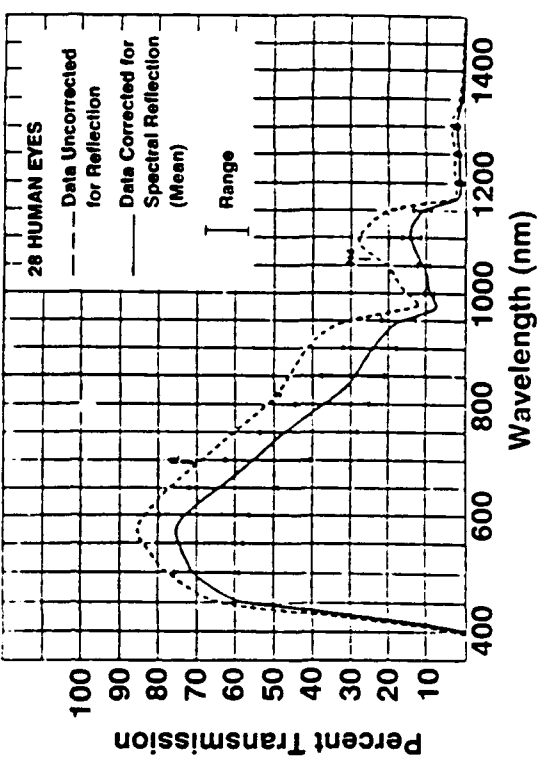
2.3 Summary Of Technical Approach

Any light that enters the eye is magnified by a factor of 10^5 at the retina. Because of this, lasers at relatively low light levels can produce substantial damage to the retina of the eye. Conventional shuttering devices, such as mechanical, acousto-optic or electro-optic techniques, have been found to be too slow relative to the rise-time of the majority of threats expected and would therefore not provide adequate protection to the eyes. Additionally, techniques such as interference filters or notch filters cannot defend against a frequency-agile threat. The consensus has been that any passive optical shuttering device would have to respond to the intensity of the light passing through the device. Nonlinear optics is an intensity-dependent phenomena and lends itself well to this application. The requirement is for the nonlinear effect to respond before the intensity builds up sufficiently to damage the eye. The difficulty with present day NLO materials is that they do not have sufficiently large NLO properties to meet this requirement. To alleviate the NLO properties requirement of the materials as much as possible, an optical lensing concept was developed and analyzed that could increase the effective NLO properties while maintaining acceptable vision.

Human Eye



Absorption in the Retina and Choroid



Transmittance of Ocular Media

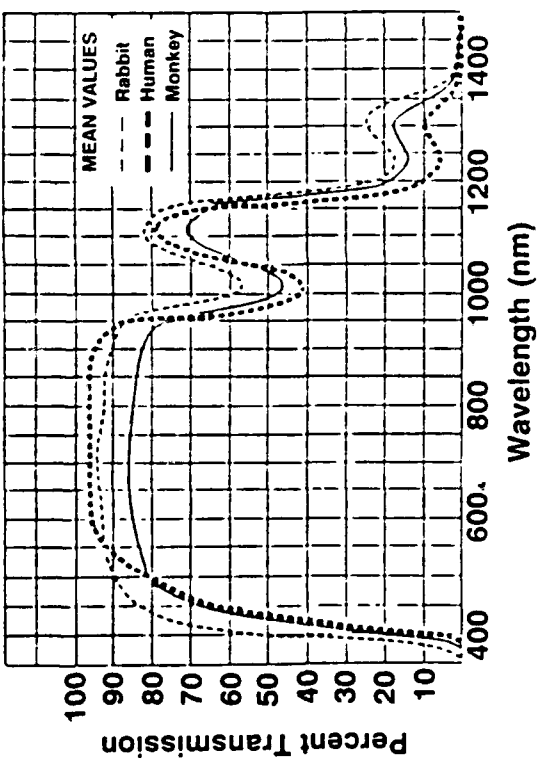
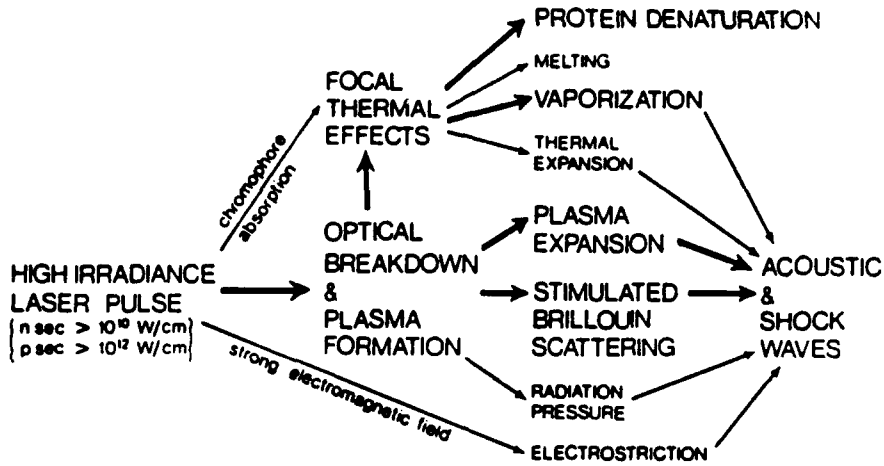


Figure 3 The Eye and Spectral Characteristics



LASER BAND	UV			VISIBLE	NEAR IR	FAR IR		
WAVELENGTH (NANOMETERS)	200	280	315	400	700	1400	3000	10 ⁶
ADVERSE EFFECTS	PHOTOKERATITIS			RETINAL BURNS		CORNEAL BURNS		
	CATARACT →			CATARACT				
	ERYTHEMA			COLOR VISION NIGHT VISION DEGRADATION				
	THERMAL SKIN BURNS							

Figure 4 Biological Effects on the Eye from Laser Radiation Exposure

The goggle eye protection device utilizes a series of four miniature lens arrays to convey a view to the eye through intermediate focal regions. Two lenslet arrays produce an inverted image. Two additional lenslet arrays are required to produce an upright image. The result is a "sandwich" structure, in which the layer of NLO material is located at each of the focal regions between the two lens arrays. The basic structure is shown in Figure 5. (The complete set of four lenses will be referred to in this report as a "quad". See Figures 40 and 41.)

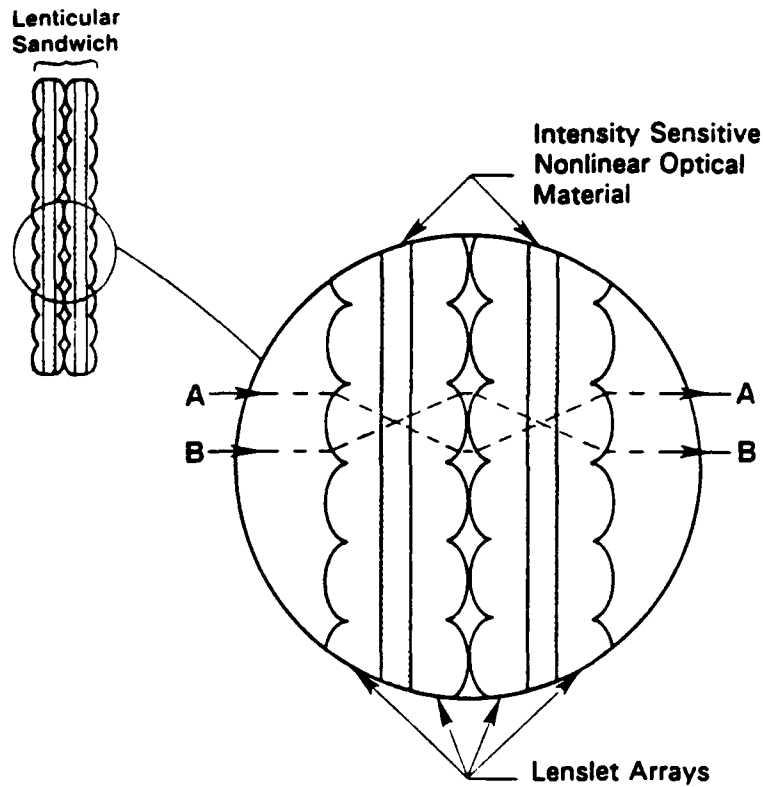


Figure 5 Schematic Representation of the Device Showing How an Upright Image Would be Transferred

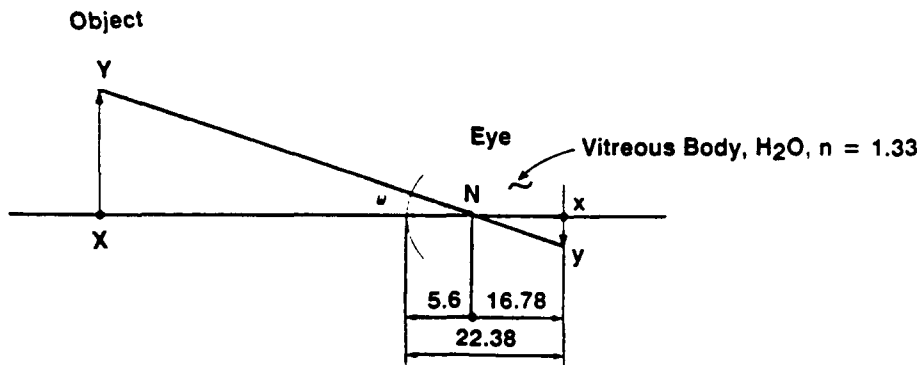
This concept has several unique features. The optical gain at each of the two intermediate focal points is in the range of 10^4 to 10^6 . These independent intermediate focal planes can be used to enhance the NLO properties of materials with potentially different wavelength responses to cover fully the visible regime, different temporal responses to respond to picosecond through CW threats, or combinations of both. This concept is also independent of the particular NLO phenomena; either passive or active phenomena can be utilized.

It is instructive to compare the advantages of a lenslet array device to a large single lens system, such as in conventional eyeglasses. The use of conventional optics in an eye protection application would result in a cumbersome, heavy device for the individual. If one considered a 4 cm diameter lens element in an $f/2$ system, the overall length of the device would be approximately 16 cm. This length is considered unacceptably large. The lenslet array concept was developed to

provide high-intensity regions in a compact structure since overall lengths on the order of 1 to 2 cm are possible using this approach. The Helmholtz model of the eye, shown in Figure 6, was used to compare and assist in the design of various lenslet types. The Helmholtz model provides a means by which to measure the effective visual acuity, field of view, and chromatic distortion introduced by the various lenslet designs. A computer modeling ray-tracing program was used for much of the analysis and provided a useful evaluation technique. A computer representation of the eye is shown in Figure 7. Some of the important parameters of the eye relevant to an optical lenslet design are shown in Figure 8 and include the modulation transfer function (MTF), visual acuity, resolution and contrast of the eye.

The technical approach used throughout this program consisted of the following steps:

- Identify relevant parameters of the eye.
- Use ray tracing analysis to develop lenslet array models.
- Model and optimize composite lenslet elements and arrays.
- Develop figure of merit criteria.
- Examine FOV issues analytically for the lenslets and the array.
- Use commercially available lenslet arrays to validate model and perform limited experiments.
- Investigate NLO requirements (cursory treatment only). A detailed NLO evaluation was beyond the scope of this current effort.
- Examine manufacturing tolerances and fabrication issues.
- Develop a prototype design.
- Fabricate prototype design.
- Evaluate optical performance of prototype design.
- Investigate manufacturing considerations.



- Radius of Curvature of Retina - 11.19 mm
- Fovea (Rod-Free Area) - $200 \mu m$ ($40'$)
- Focal Length - 16.84 mm

Figure 6 Helmholtz Model of the Eye⁽¹⁾

N = nodal point
 n = index of refraction
 ω = visual angle

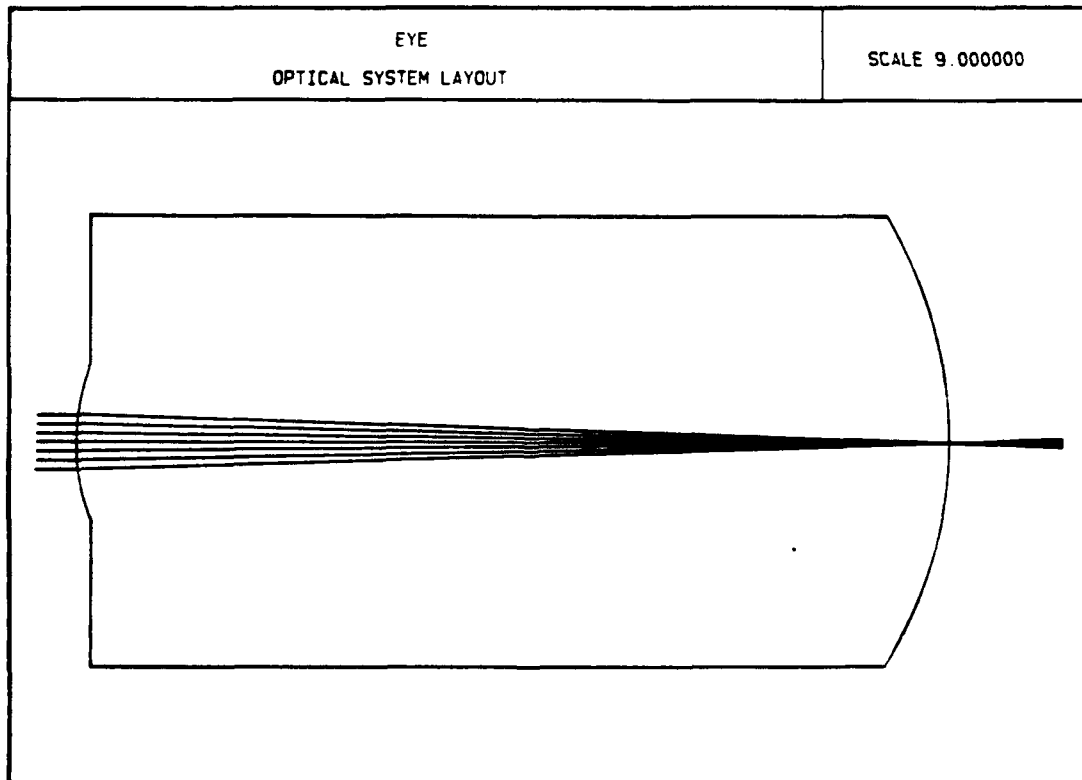
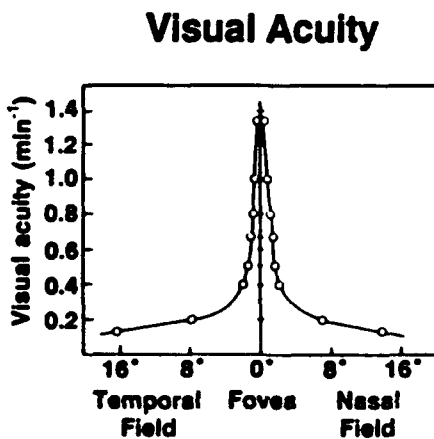
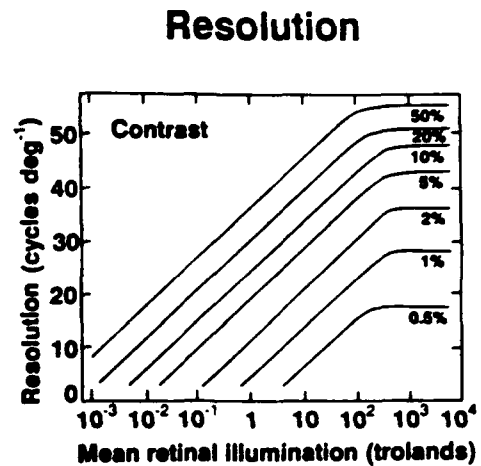
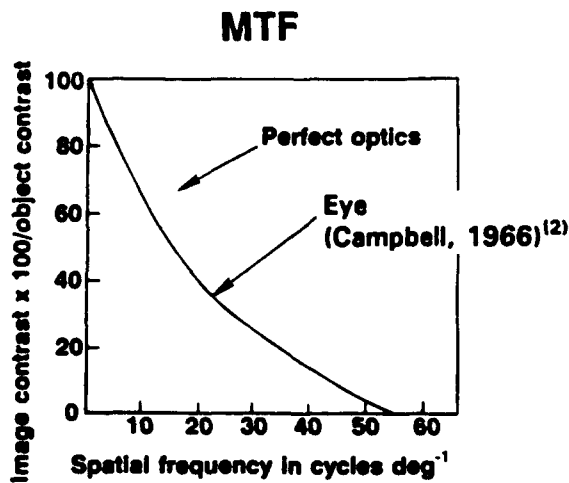


Figure 7 Computer Schematic of the Eye Model



Troland

Retinal Illuminance

1 Troland = 1 nit/mm²

1 nit = 1 lumen/steradian/m²

1 watt = 673 lumens @ 555 nm

Figure 8 Modulation Transfer Function (MTF), Resolution, and Visual Acuity of the Human Eye

2.4 Summary Results Of Phase I

During Phase I, the following investigations were performed:

- A basic procedural analysis capability was developed using Super-Oslo™, an optical ray tracing program, to evaluate the on-axis performance of several lenslet types.
- Relevant parameters of the human eye were investigated and incorporated into the Super-Oslo model. This provided a mechanism for comparing the optical performance of the various lenslet designs.
- An evaluation criterion was developed along with a relative ranking that could be used to indicate the potential viability of a particular lenslet design.
- A commercially available lenslet array was experimentally evaluated and compared with the theoretical models.

- A parameter space was explored that included such variables as lenslet diameter, f-number, package length, and optical gain.
- Various lenslet packing configurations were investigated including those that utilized square, round and hexagonal lenslet quads.
- Preliminary assessment of lenslet fabrication technologies and mechanical tolerances were explored.

Conclusions of Phase I:

- High quality imagery was achievable.
- Three lenslet designs needed further optimization: aspheric, curved GRIN, and kinoform with spherical.
- The theoretical modeling performed was reasonably correct.
- Packing of the lenslets into a hexagonal array appeared best.
- The FOV issue appeared resolvable.
- State-of-the-art fabrication technologies would be required.

2.5 Summary Results Of Phase II

During Phase II, the following investigations were performed:

- Optical analysis was extended to include nonidentical lenslet elements within a quad configuration.
- Optical analysis was extended to off-axis performance evaluation.
- Investigation was performed to determine the viability of using kinoform technology (binary optics) as a stand-alone optical system without any refractive elements.
- The FOV of some lenslet arrays was investigated.
- The potential for the lenslet array to produce multiple images on the retina of the eye was investigated.
- Preliminary nonlinear optical phenomenologies were investigated for possible future incorporation into the lenslet array.

Conclusions of Phase II:

- High quality imagery was still believed achievable.
- Complex lenslet elements provided high acuity vision on-axis with a moderate FOV.
- The necessary FOV could be obtained by curving the lenslet array.

- Significant effort would still be required to determine the feasibility of utilizing nonlinear optical materials within the lenslet concept to protect the eyes. (This effort was considered beyond the scope of the current program.)
- Stand-alone kinoform technology (binary optics) would not provide a solution to this problem.
- Kinoform elements in conjunction with refractive elements were a viable solution but possibly not the most cost effective.

2.6 Summary Results Of Phase III

During Phase III, the following investigations were performed:

- A specific optical design (PROTO90Q) was developed, to be reduced to practice, under this program.
- The optical gain at the first focal point for various angles of incidence was investigated.
- A spherical lenslet eyepiece was designed and fabricated and mounted in the U.S. Army Sun, Wind and Dust Goggle frame.
- A Humphrey field analyzer was used in conjunction with a human subject to determine any FOV restriction in the design of the lenslet eyepiece.
- Fabrication of lenslets, using an injection molding process, was initiated with Plastec, Inc.

Conclusions of Phase III:

- An optical design existed that could provide reasonable visual acuity and FOV within a reasonable package size.
- Significant work remained to eliminate the current restrictions on the orbital motion of the eye.
- While the lenslet concept appears viable, much work remains on a number of engineering and optical design issues.

2.7 Summary Results Of Phase IV

During Phase IV, the following investigations were performed:

- The injection molding processes of several lenslet manufacturers were investigated.
- The PROTO90Q design was fabricated and its optical quality experimentally evaluated.
- An array consisting of 19 quads, 4 lenslets/quad, was constructed. The complete device consisted of 76 lenslet elements.
- Initial estimates were made for both the recurring and nonrecurring costs associated with quantity production of the lenslet goggle device.

Conclusions of Phase IV:

- **The optical quality of the PROTO90Q lenslets received from Plastec, Inc., was very poor. After several fabrication iterations the subcontract with them was cancelled. They were unable to meet the optical design requirements.**
- **Significant information was obtained from Plastec, Inc., concerning the assembly of the lenslet array.**
- **OPKOR, Inc., subsequently fabricated the first lenslet of the PROTO90Q design.**
- **The lenslets received from OPKOR, Inc., were of very high optical quality. OPKOR, Inc., was able to meet the optical design requirements.**
- **The lenslet array, fabricated using the OPKOR, Inc., lenslet elements, showed moderate optical quality when evaluated visually.**
- **Initial manufacturing estimates indicate a cost of \$1,000 - \$2,500/goggle device. Further refinement of these estimates will be required.**

3.0 PHASE I EFFORTS

The approach taken throughout this investigation was to start with commercially available optical lenslets, assess their viability for incorporation into the eye protection device, and then, if the desired level of optical performance was not achieved, extend the analysis to lenslets not commercially available. The initial investigation under Phase I restricted the four lenslets used in each element to a single lenslet type. The intent was to keep the design as simple as possible and thereby produce a cost-effective goggle device. Different lenslet types, within a quad configuration, were investigated during Phase II.

3.1 Lenslet Types Evaluated

During Phase I, various lenslet types were evaluated theoretically using Super-Oslo, a ray tracing program. For this first analysis, only on-axis performance was considered and attempts were made to achieve diffraction-limited performance with the restriction that all four lenslets in a row were identical. Table 1, along with Figures 9 through 17, provides a summary of this analysis.

Four of these initial lenslet types were identified as potentially viable for the lenslet array eye protection concept. These were the aspheric, curved GRIN, combination kinoform and spherical lenslet and the refractive achromat. All demonstrated near-diffraction limited performance on-axis and were realizable with currently available manufacturing technology, with the possible exception of the binary optic design (kinoform optics).

Binary optics are extremely wavelength sensitive and only work well at the design wavelength. Recently, a wavelength independent grating lens system was reported that had an allowable wavelength range of $\pm 15 \text{ nm}^{(3)}$. This technique was investigated, resulted in only minimal success, and was not pursued further.

Table 1 Summary of Lenslet Types Evaluated

Lenslet Type	On-Axis Optical Performance Shown in Figure	Comment(s)
Spherical-Plano	9	Commercially available from Aeroflex Laboratories, Inc. These lenslet arrays (Series MRP-100) were made from acrylic plastic and were 2.25 x 2.25 x 0.204 inches in size. The individual lenslets were square with dimensions of 0.043 x 0.043 inches with an effective aperture of f/3.0.
Aspherical-Plano	10	Not commercially available optical design theoretically modeled to provide diffraction-limited performance on-axis.
Plano-GRIN	11	GRIN (gradient index) lenslets commercially available from Melles Griot.
Spherical-GRIN	12	Commercially available from Melles Griot.
Spherical-GRIN	13	Not commercially available. Optical design theoretically modeled to provide near diffraction-limited performance on-axis.
Spherical-Ball	14	Commercially available from Melles Griot.
Kinoform (binary optical element)	15	Not commercially available. Optical design theoretically modeled to provide diffraction-limited performance on-axis.
Kinoform-Aspherical Lens	16	Not commercially available. Optical design theoretically modeled to provide diffraction-limited performance on-axis.
Refractive Achromat	17	Not commercially available. Optical design theoretically modeled to provide chromatically corrected diffraction-limited performance on-axis.

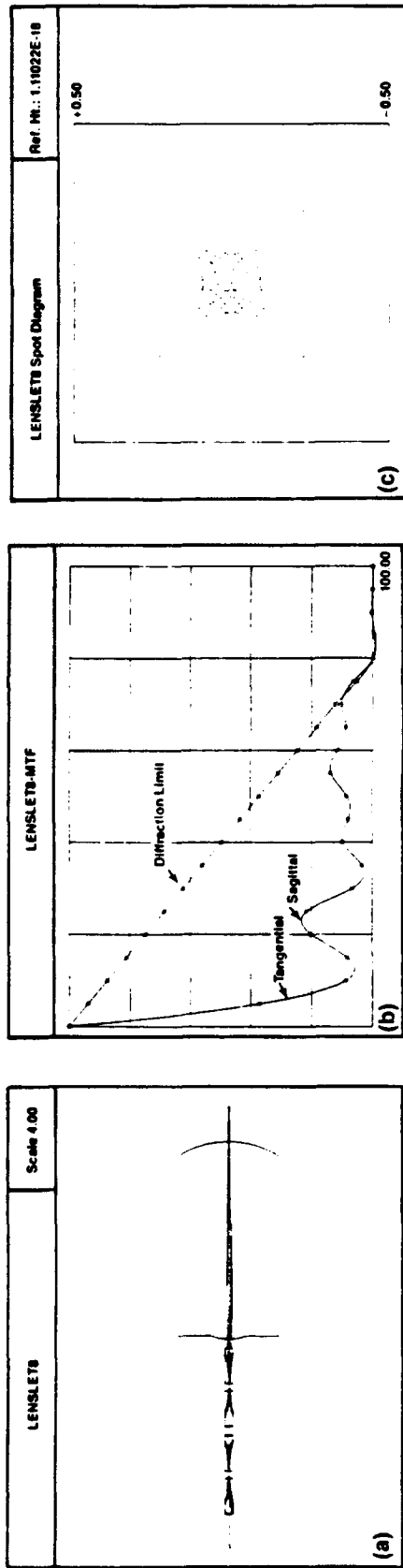


Figure 9 Commercially Available Spherical Lens, Aeroflex
 (a) Ray Trace, (b) Modulation Transfer Function (MTF),
 (c) Spot Diagram, Range is ± 0.5 mm

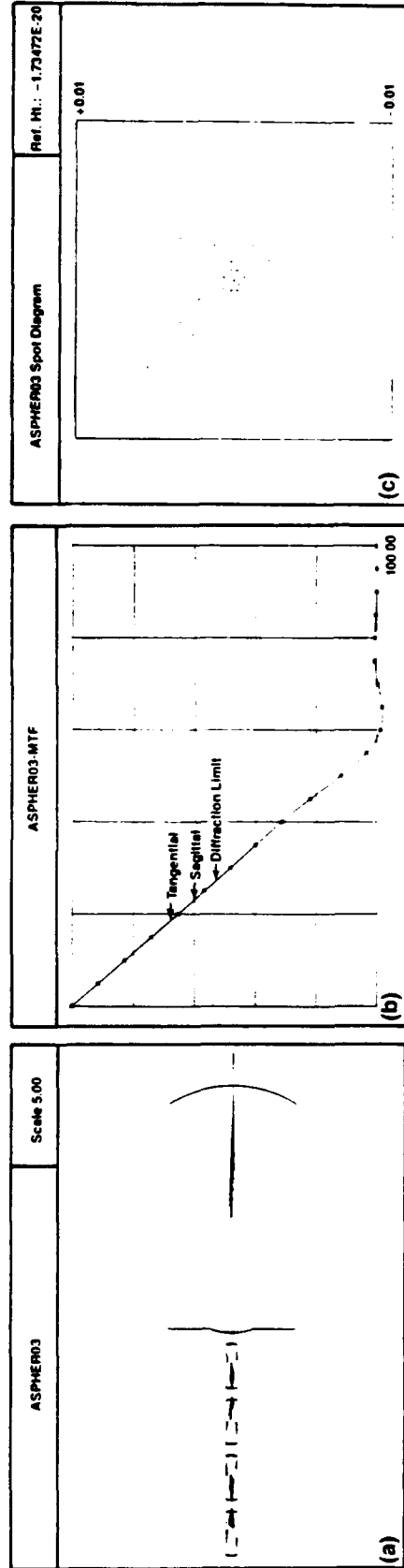


Figure 10 Modified Aeroflex Lens with Aspherical Surface
 (a) Ray Trace, (b) MTF, (c) Spot Diagram, Range is ± 0.01 mm

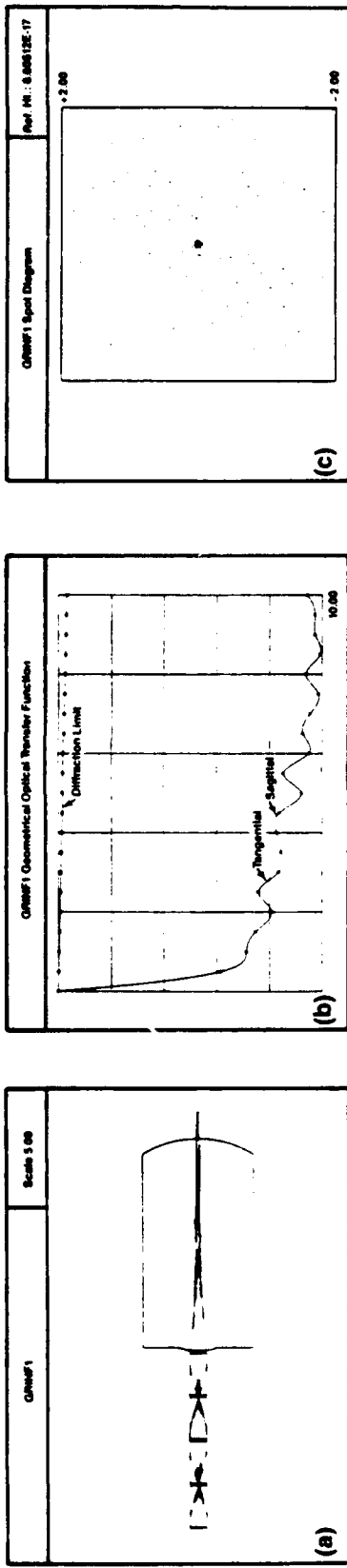


Figure 11 Commercially Available Flat Surface GRIN Lens, Melles Griot: (a) Ray Trace, (b) Geometric Optical Transfer Function (GOTF) (System Performance is too Aberrated to Calculate the MTF), (c) Spot Diagram, Range is ± 2.0 mm

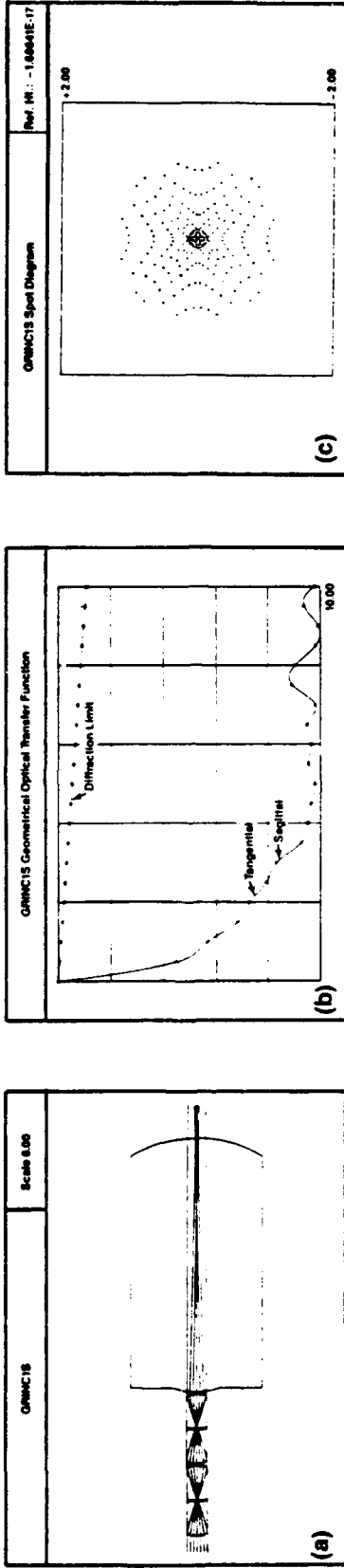


Figure 12 Commercially Available Spherical Surface GRIN Lens, Melles Griot (a) Ray Trace, (b) GOTF, (c) Spot Diagram, Range is ± 2.0 mm

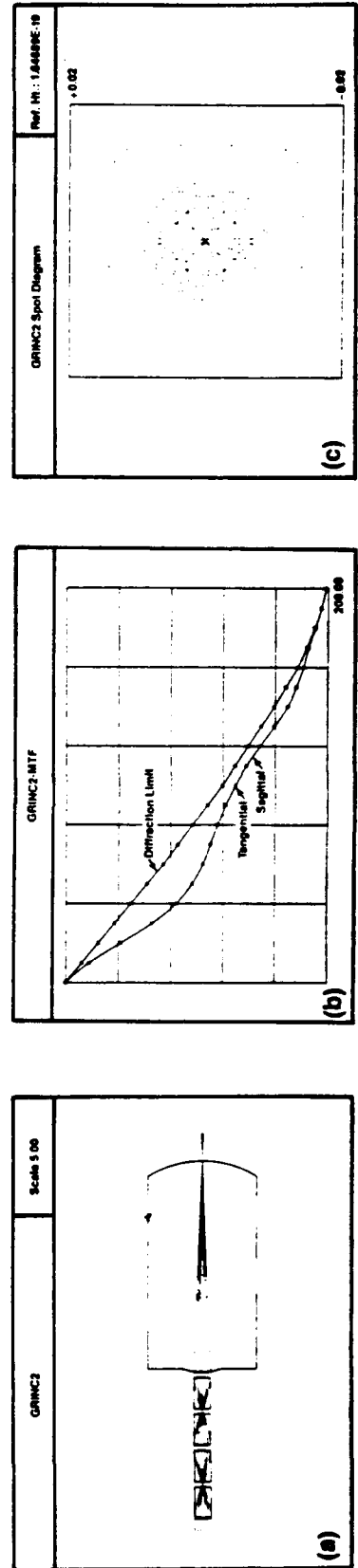


Figure 13 Modified Melles Griot Spherical Lens with Conjectured Curvature (a) Ray Trace, (b) MTF, (c) Spot Diagram, Range is ± 0.02 mm

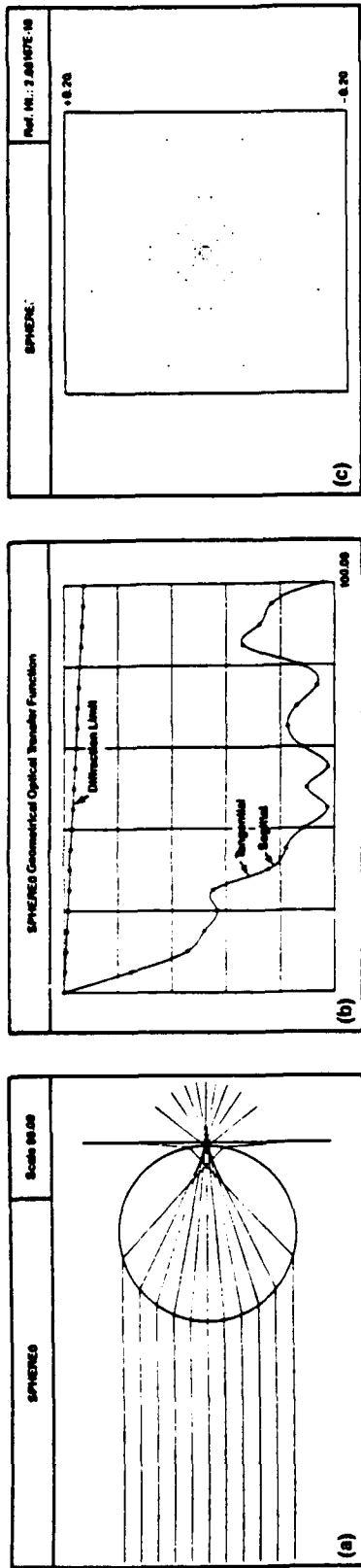


Figure 14 Commercially Available Spherical Ball Lens, Melles Griot
 (a) Ray Trace, (b) GOTF, (c) Spot Diagram, Range is ± 0.2 mm

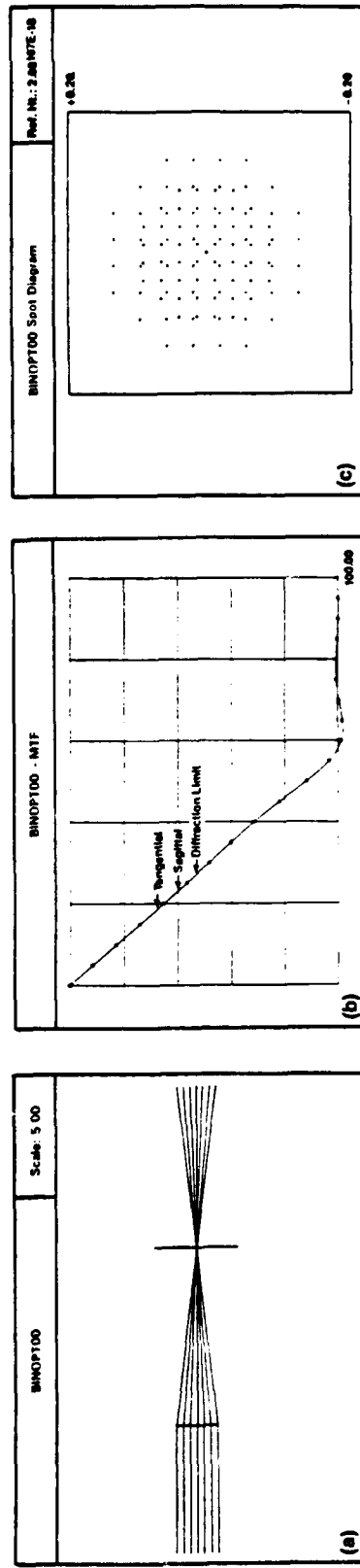


Figure 15 Binary Optical Element: (a) Ray Trace, (b) MTF, (c) Spot Diagram, Range is ± 0.20 mm
 (At design wavelength, all rays focus to a single point. Large spot diagram is due to all other wavelengths in the visible regime.)

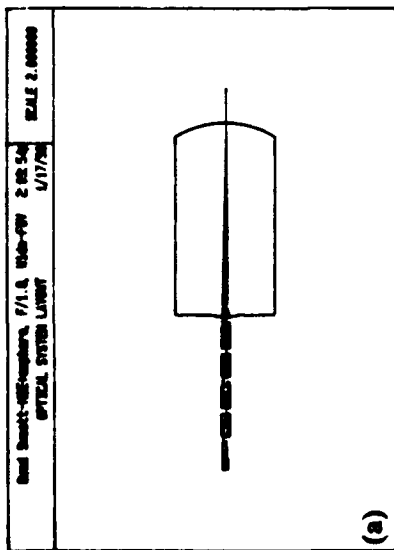
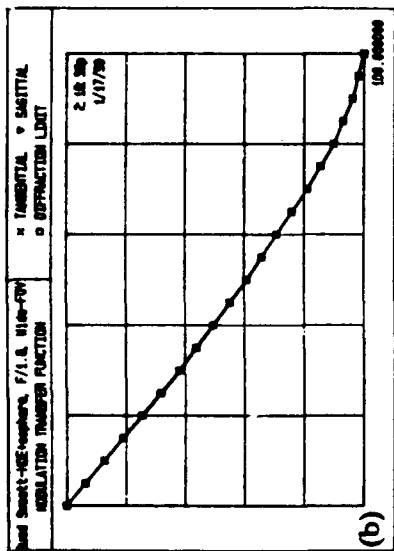
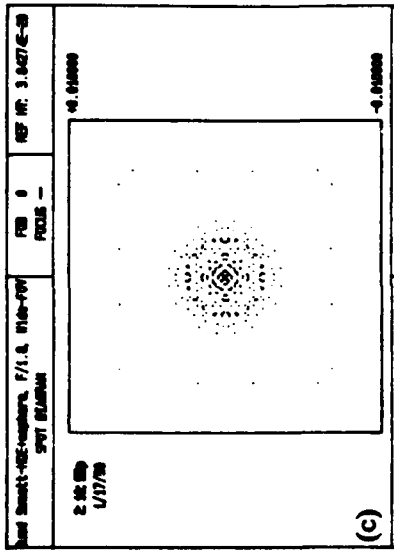


Figure 16 Kinoform with Asphere Design
(a) Ray Trace, (b) MTF, (c) Spot Diagram, Range is ± 0.01 mm

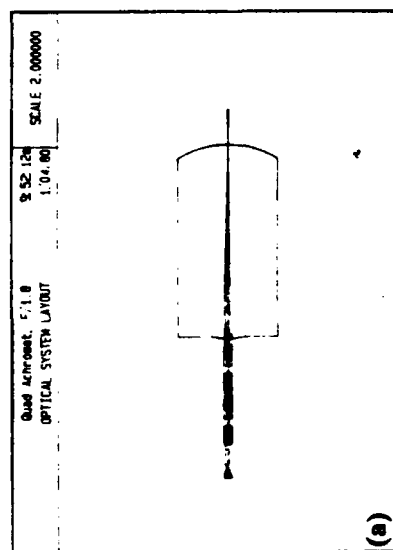
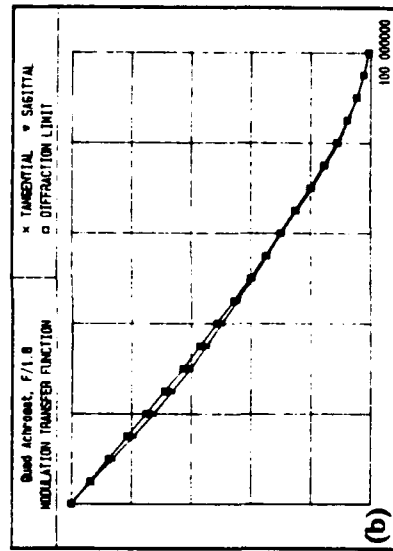
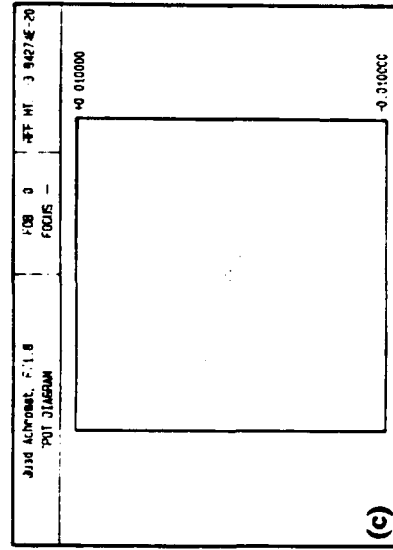


Figure 17 Refractive Achromat Design
(a) Ray Trace, (b) MTF, (c) Spot Diagram, Range is ± 0.01 mm

3.2 Experimental Verification of Model

The methodology used to model the lenslet elements was validated experimentally using the spherical Aeroflex lenslet arrays. A test station was established, shown in Figure 18, so that the lenslet arrays could be assessed in terms of their visual performance. Four one-inch squares of the Aeroflex lenslet arrays were paired to make separate right and left lenslet eyepieces in order to represent two-eyed goggles so that binocular as well as monocular visual evaluations could be made. Only single pairs of lenses (half-quad unit) were set up for each eye instead of double pairs (quad unit). Both ray-tracing predictions and quick visual examination of performance indicated that the aberrations of double pairs would have been too severe to allow any practical assessment of performance. Since the aberrations are multiplicative for identical elements in an afocal arrangement, these doublets showed much lower aberration and therefore allowed visual assessment of the imaging capabilities.



Figure 18 Test Station for Optically Evaluating Lenslet Arrays

The individual one-inch squares were mounted mechanically so that one element of each binocular pair was stationary while the companion element could be precisely adjusted through six degrees of freedom. Initial evaluations were made visually and photographically. A standard Air Force 3-bar target was set up 184 cm in front of the goggles. Figure 19 shows a direct photograph of the target taken with a 50-mm lens at an aperture stop of $f/16$, which is equivalent to an aperture diameter of 3.1 mm. Figure 20 was taken the same way but through one of the lenslet pairs. Although the general features of the target are obvious, the resolution is poor. This poor performance, however, is in quantitative agreement with the ray-trace model of lenslet elements with spherical surfaces. Visual assessment through one array pair yielded a limiting resolution of roughly 17 cycles/mm (4.9 cycles/degree) and a binocular resolution of about 20 cycles/mm (5.8 cycles/degree). The 50% MTF contrast level corresponded to a monocular resolution of about one-half the limiting resolution of 8.5 cycles/mm. The performance predicted by Super-Oslo was 8.0 cycles/mm and was in good agreement with the experiment. The photographs recorded the same level of performance. Measurements without the lenslet pairs in the experimental set-up yielded a monocular visual resolution limit of 90 cycles/mm. The spherical lenslet pairs therefore reduced the resolution by a factor of five.

3.3 Lenslet Array Packing Configurations

Three lenslet packing configurations were investigated to determine the most effective configuration for assembling the individual lenslet quads into a pair of goggles. Minimization of the combined spot size was the only criteria used for determining the "best" configuration. The three geometries considered were square lenses in a square grid, circular lenses in a square grid, and circular lenses in a hexagonal grid as shown in Figure 21. In the first configuration, no area is lost between adjacent lenslets, whereas, in the second and third configurations, 21% and 9%, respectively, of the array surface area falls between lenslets.

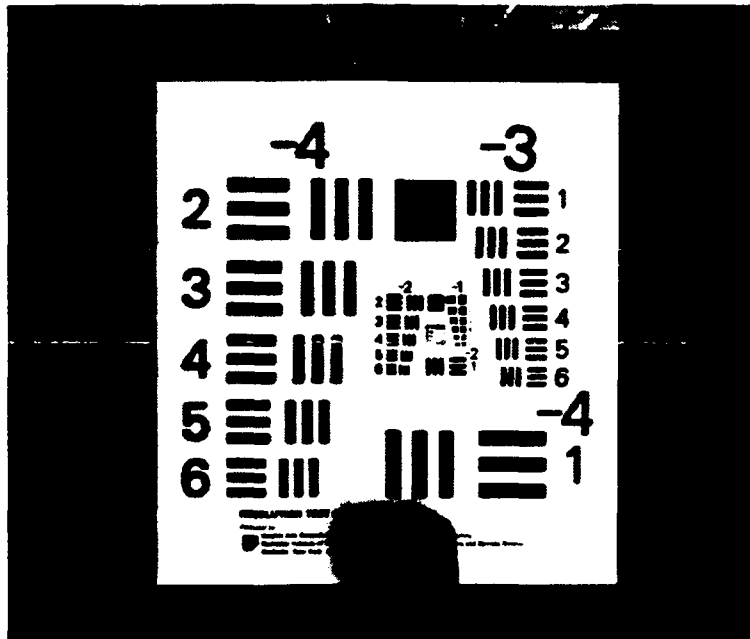


Figure 19 Naked Eye Resolution

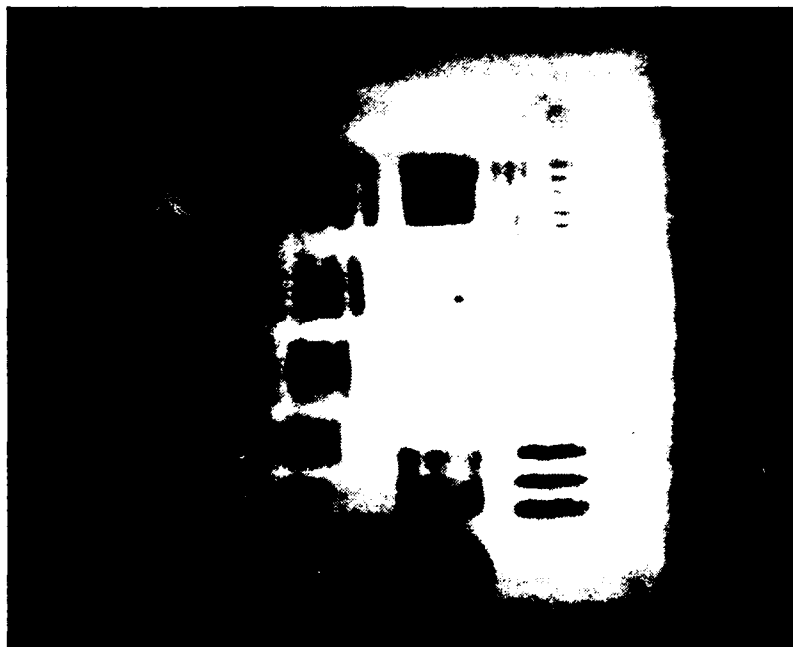


Figure 20 Single Pair Aeroflex Lenses Resolution

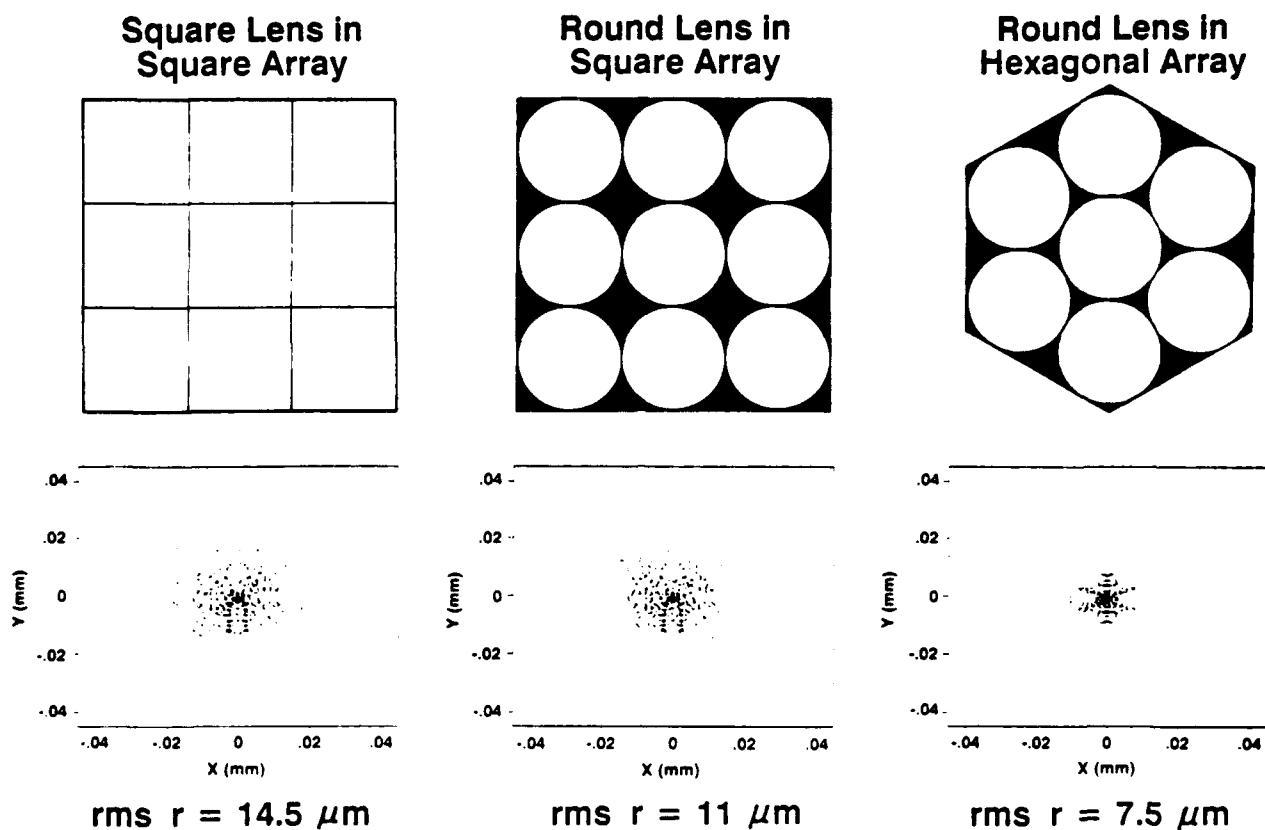


Figure 21 Array Geometry Spot Diagrams
rms r = radius of root mean square
average spot size

Although the square lens/square grid configuration has the highest transmission factor, it has the worst composite spot diagram, also shown in Figure 21. The best performance occurs in the circular lens/hexagonal grid configuration. Performance of the circular aperture is superior to the square aperture because it has a larger portion of its area close to the optic axis. This minimizes aberrations that tend to grow rapidly off-axis. In addition, the close-packing and the higher degree of symmetry of the hexagonal array contribute to the compact, more circular composite spot, and consequently, to better optical resolution. Currently, therefore, an array configured with round lenses in a hexagonal array appears optimum.

3.4 Ghost Images on the Retina of the Eye

In the design of a monolithic lenslet array, such as the Aeroflex array, when the angle of the incident light exceeds the maximum acceptable angle for a single lenslet, the light ray can be passed to a lenslet above or below the one it entered - this gives rise to secondary, or ghost images. Ghost images can be generated by the lenslet array as shown in Figure 22. When paraxial light rays enter a lenslet near its edge, the rays should, in principle, exit the second lenslet near its edge. If the rays are not exactly parallel to the optic axis, they may exit through the curved surface of an adjacent lenslet instead of the appropriately paired lenslet. The actual exit surface's curvature and the ray's angle of incidence on it are such that the refracted ray travels further off-axis. These rays are focussed by the eye producing a secondary image on the retina far from the fovea. The eye then sees the poorly focussed images as well as the main image formed by the well-behaved light rays. Ghost images were in fact observed experimentally in the Aeroflex design. A sketch of the scene observed is shown in Figure 23. Cross-talk between adjacent lenslets must be prevented in order to eliminate the unwanted images. The individual lenslet elements must be isolated so that light rays entering a particular lenslet can exit only from that quad. The isolation can be achieved by manufacturing an effective shield around the length of the lenslets. GRIN lenses have this feature inherently due to the gradient index structure of the device.

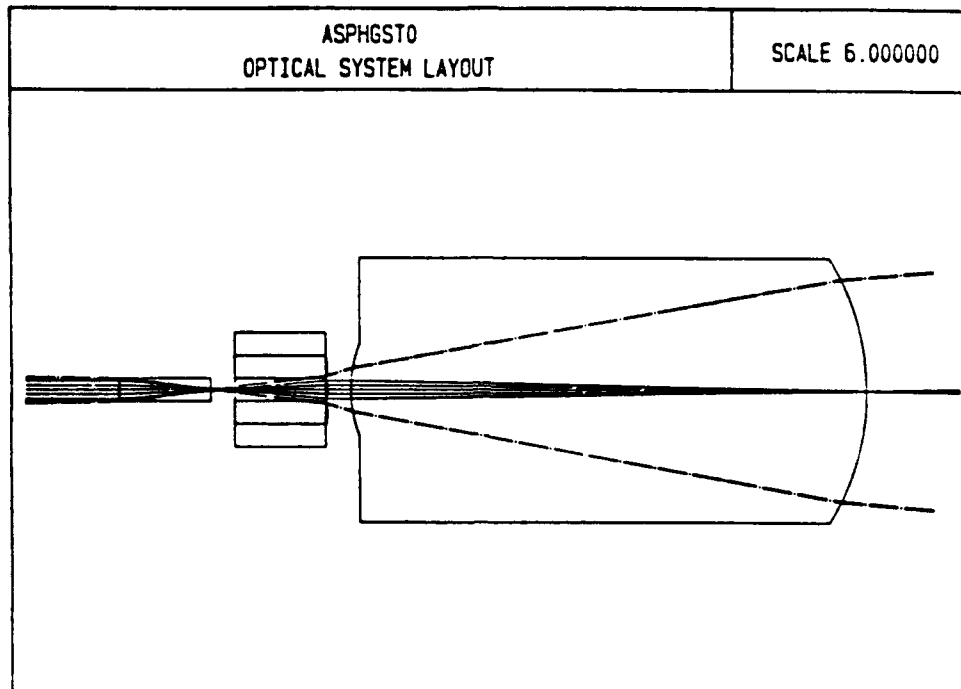


Figure 22 Ghost Images
 Rays at upper and lower edges of aperture are $\sim 1^\circ$ off-axis

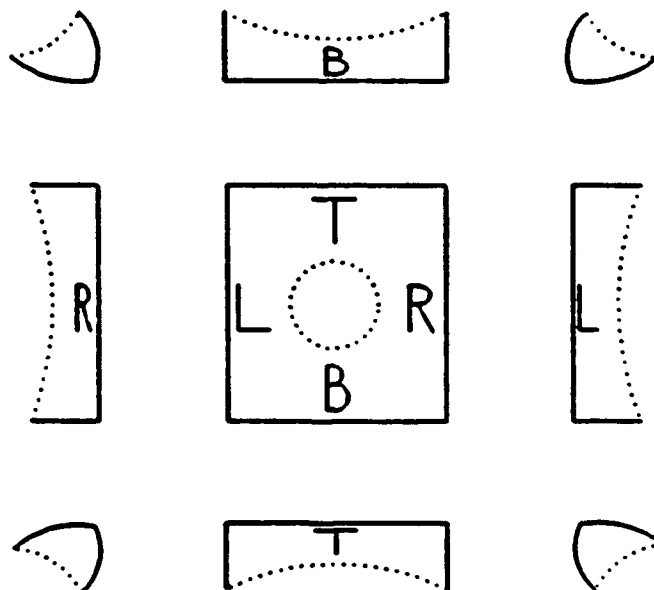


Figure 23 Sketch of First-Order Ghosts Visible in Paired-Aeroflex Experiments
 (T = Top; B = Bottom; L = Left; R = Right)

4.0 PHASE II EFFORTS

4.1 Off-Axis Performance Characteristics of the Lenslet Elements

Only the lenslet elements that showed good on-axis performance continued in the evaluation process of off-axis performance. Each of these designs, excluding the achromatized kinoform, had certain attributes associated with them that warranted further investigation. The performance of each combination was optimized, through an iterative process, for polychromatic operation at red, green, and blue wavelengths as well as over a radial 1-degree FOV. The performance was then predicted over a radial 5-degree FOV. Figures 24 through 28 show graphically the predicted spot radius on the retina for the various quad configurations. The f-number for the asphere refractor design, shown in Figure 24, was kept at a value of $f/2$ to provide continuity with the previous analysis of the asphere and actually shows better performance than had an $f/1.8$ system been evaluated.

The spot sizes for these graphs were plotted on a logarithmic scale so that the performance differences between the various designs could be easily observed. Figure 24 shows the differences between the refractive aspheric design and the combination kinoform with spherical lens design for both monochromatic and polychromatic operation. While the performance of the asphere is relatively flat out to 1 degree, the on-axis performance of the kinoform with sphere is near diffraction-limited but quickly degrades to a level equivalent to the performance of the asphere. Figure 25 takes the kinoform with sphere and compares it to a kinoform with asphere; notice the vertical scale change. The performance of the kinoform with asphere is substantially superior to the kinoform with sphere. Both the monochromatic and polychromatic behavior of the kinoform with asphere remain essentially diffraction-limited out to an angle of 1 degree. Figure 26 has another scale change and compares the kinoform with asphere to an aspherically curved GRIN lens. Once again there is an improvement in performance. The aspheric GRIN shows near-diffraction-limited performance out to 3 degrees.

A summary of these four designs is shown in Figure 27. This graph presents all the information on the same scale and is useful in comparing the improvements resulting from each design.

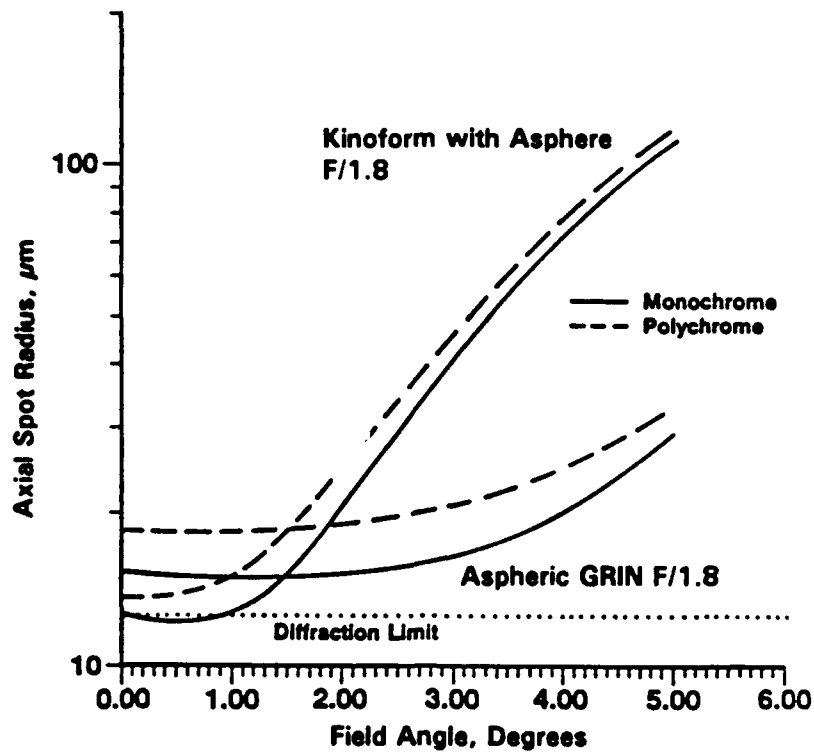


Figure 24 Optical Performance of the Quad Asphere and the Quad Kinoform with Sphere as a Function of Field Angle

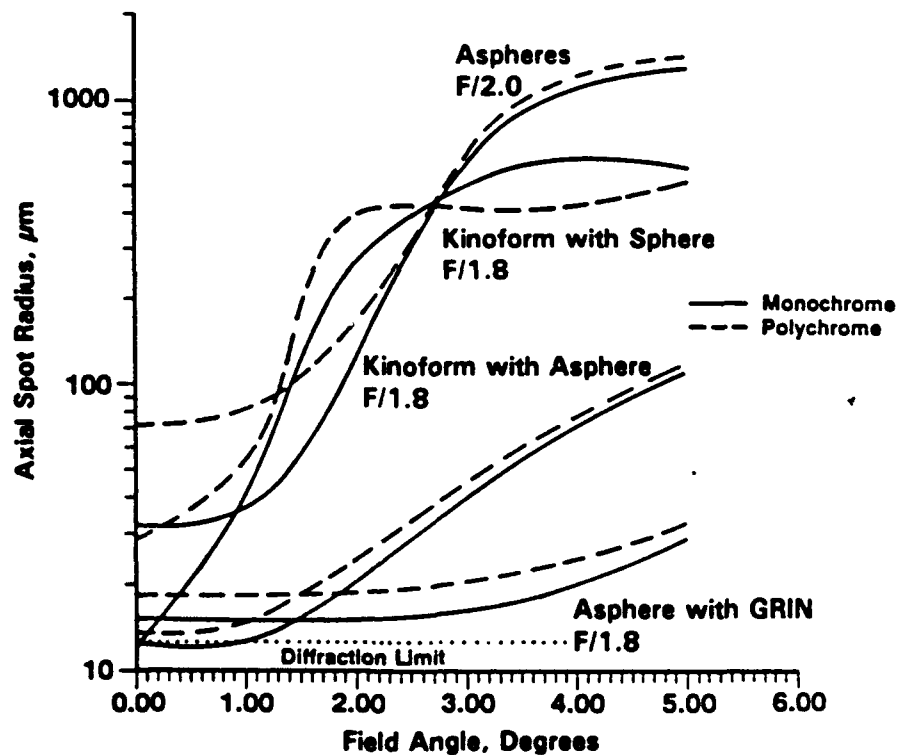


Figure 25 Optical Performance of the Quad Kinoform with Sphere and the Kinoform with Asphere as a Function of Field Angle

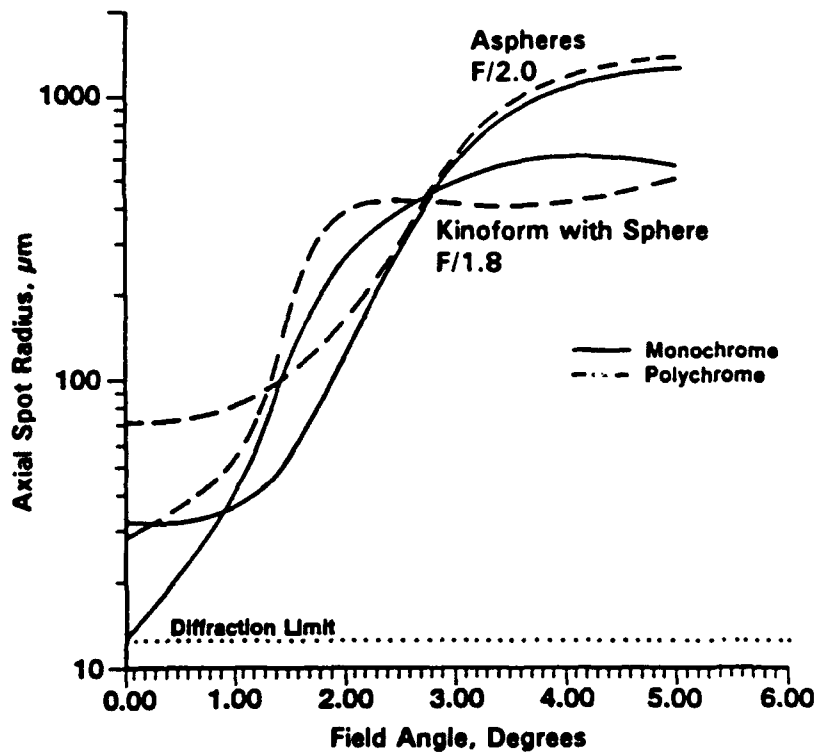


Figure 26 Optical Performance of the Quad Kinoform with Asphere and the Aspheric GRIN as a Function of Field Angle

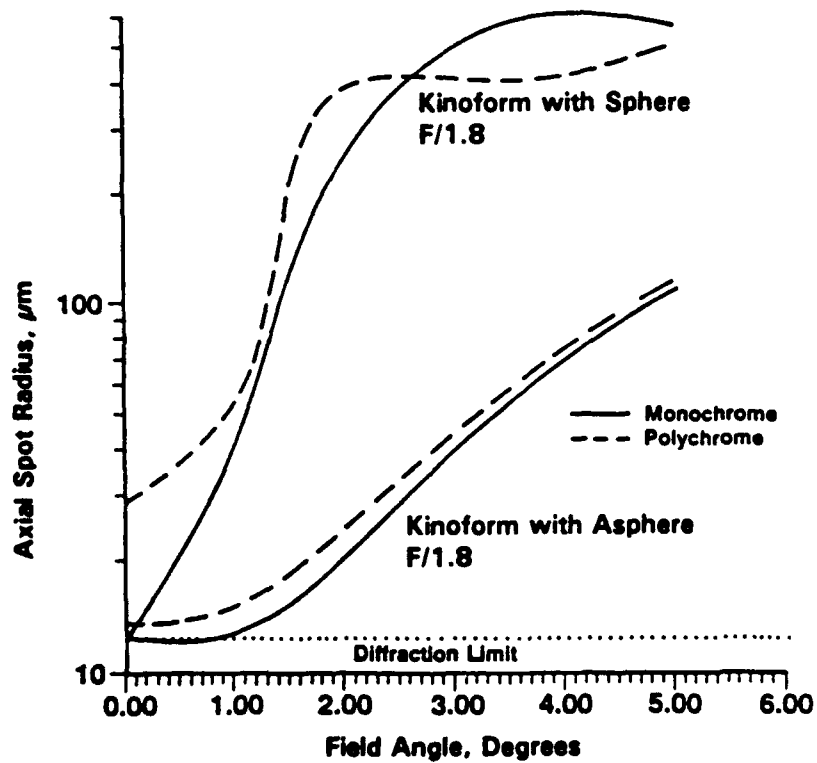


Figure 27 Optical Field Angle Performance Summary of Four Quad Lenslet Designs

Figure 28 shows the performance of the dual plastic achromat in comparison to the previously discussed designs. While not quite as good as the other two designs, it still shows reasonable performance. The performance of this refractive achromatic design might be improved by removing the restriction of a spherical interface between the two plastic elements and by allowing a nonplanar rear surface.

From the above analysis, it appears evident that while diffraction-limited performance can be obtained for the quad units over a limited FOV, it cannot encompass very many degrees without substantially reduced performance. The high-acuity region of the eye only has a $\pm 1/3$ degree FOV so a logical question in evaluating the off-axis performance of the lenslets is "How good is good?". To address this issue, we considered the aspheric quad unit which has already been shown to have poor off-axis performance in comparison to other designs. Figure 29 shows experimental data on the visual acuity of the eye as a function of the FOV angle⁽⁵⁾. Superimposed on this is shown the theoretically modeled data of an $f/3$ and $f/4$ aspheric system. The results indicate that only minor degradation, if any at all, occurs several degrees off-axis and that the high-acuity region is unimpaired.

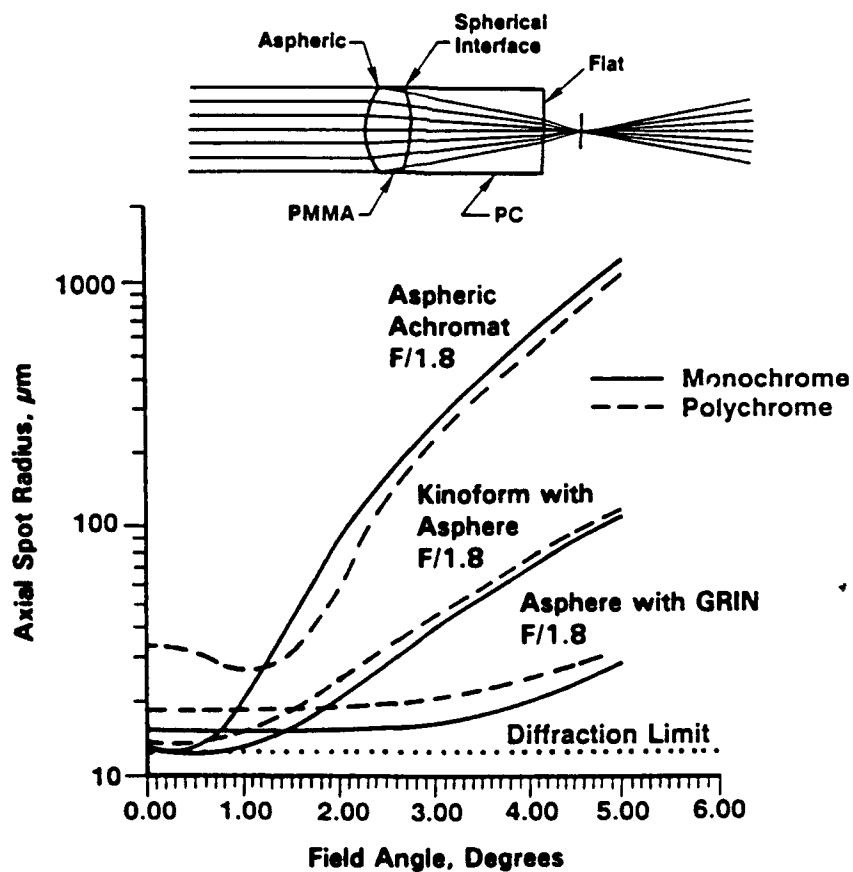


Figure 28 Optical Performance of the Aspheric Achromat as a Function of Field Angle

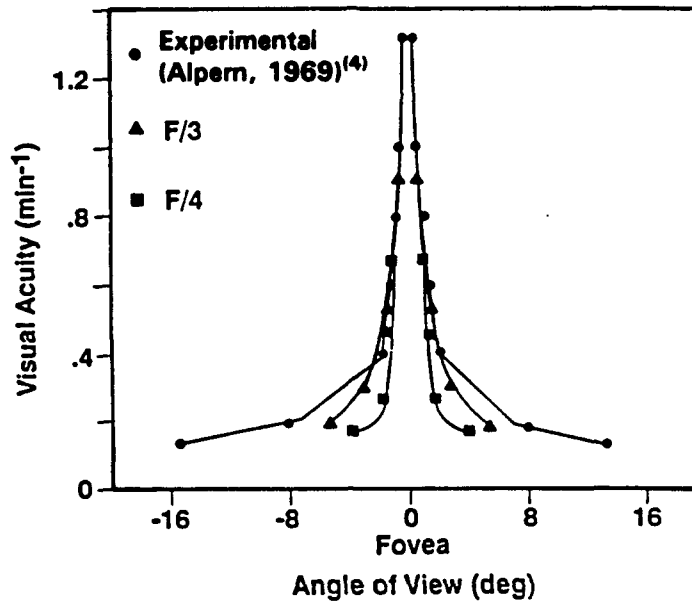


Figure 29 Comparison of Visual Acuity for Human Eyes and the Aspheric Design as a Function of Field Angle

4.2 Optical Engineering Guidelines

Engineering guidelines were established to assist in understanding the interrelationships and trade-offs of the various parameters involved in designing the lenslet array. Figure 30 shows an analysis for a diffraction-limited lenslet. The solid lines represent a family of curves with the f-number of the lens as the parameter and relate the gain of the optical system at the focal point to the lens diameter. The dashed lines represent a family of curves with the overall device thickness as the parameter. The intersections of the solid and dashed lines represent possible operating points and relate the lenslet diameter to the optical gain. For example, if one assumed a maximum device thickness of 12 mm and an $f/2$ optical system then the lenslet diameter would be approximately 1.4 mm and the device would have an optical gain of approximately 3×10^5 . The enclosed triangular region represents the approximate operational parameter space for most realistic devices. Similar graphs for actual designs of an aspheric and a curved-GRIN lens have also been developed. These graphs show that for lenslet diameters between 1 to 4 mm, optical gains between $10^5 - 10^6$ should be obtainable.

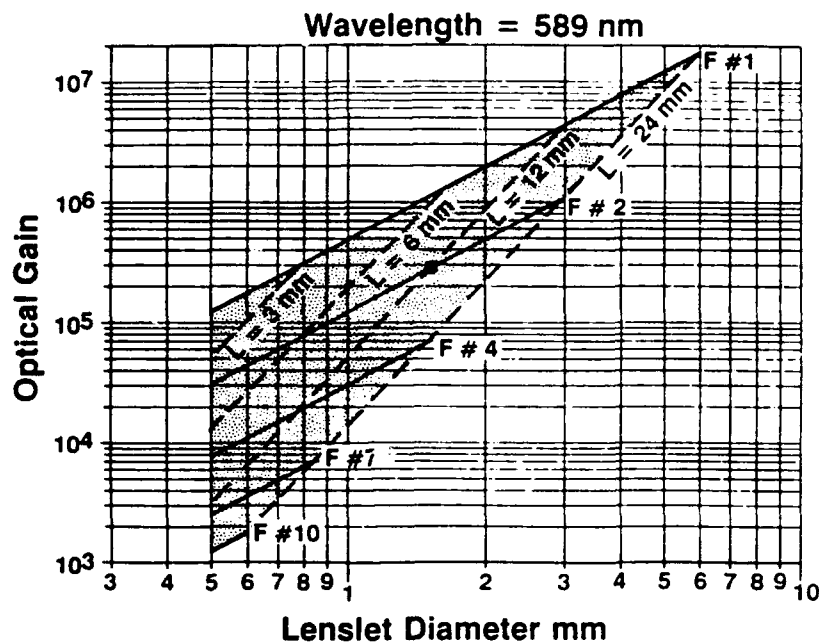


Figure 30 Design Parameter Space

4.3 Preliminary Nonlinear Optical Phenomena Assessment

The majority of nonlinear-optical device concepts for eye and sensor protection are based on the idea of self-focusing or self-defocusing of an intense beam. The basic phenomenon involved is that of the nonlinear refractive index. The refractive index of any material in which an optical beam is propagating can be written in the form

$$n = n_0 + n_2 I$$

where, I is the beam intensity and n_0 is the usual refractive index measured using light of low intensity. The nonlinear refractive index, n_2 , may be either positive or negative. Like the usual refractive index, it depends on the wavelength of the light involved and in crystalline or oriented media on the direction of light propagation. Unlike the usual refractive index, it depends on the polarization state of the light, even in isotropic media. At the nanosecond level and longer, many effects can contribute to the nonlinear index, including molecular reorientation, creation and response of free carriers, and response of delocalized electrons such as occur in conjugated bonds. If a material is absorptive, and the absorbed energy is converted into heat, then an effective n_2 equal to $(dn_0/dT)\Delta T$ may be observed if the optical pulse length is long enough, or the pulse repetition rate is high enough, compared to the thermal energy dissipation time. In some materials, simultaneous

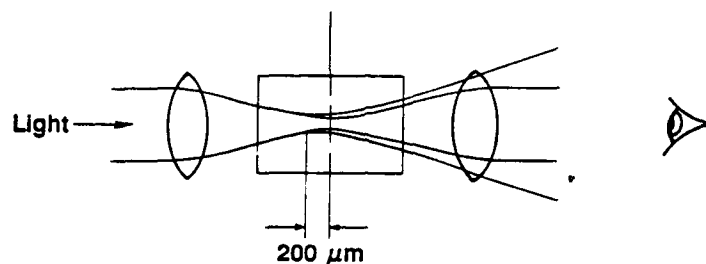
absorption of two photons in a spectral region ordinarily considered transparent at low light intensities has been shown to lead to nonlinear refractive effects. In this and quite a few other cases, the nonlinear refractive index may exhibit what amounts to an intensity dependence of its own. Collective phenomena on the molecular level, such as the massive molecular reorientation that may be induced in liquid crystals, are generally considered to be too slow to be used in devices that must respond on nanosecond time scales.

If a beam with an initially uniform phase front has an inhomogeneous cross section, such as a Gaussian beam, and is propagating in a medium with a positive nonlinearity, then regions near the center of the beam will encounter a higher refractive index, and thus have a lower phase velocity, than those near the edges; from Huygens' principle one can see that this will lead to a tendency for rays to bend toward the high-intensity region. If the intensity is high enough to overcome the natural tendency of the beam to have diffractive spreading, then the material will act like a positive lens; that is, self-focusing of the beam will occur. If the focal point of the induced lens is within the nonlinear medium, and the power is high enough, breakup of the beam into a chaotic array of very high intensity filaments may take place. It is generally believed wise to avoid this regime in order to prevent permanent physical damage to the optical medium. If a medium has a negative n_2 , then defocusing of an externally focused beam can take place at high light intensities in a similar way. The experimental facts and theoretical analysis of whole-beam planar-phase-front self-focusing were reviewed some years ago by Shen⁽⁵⁾ and by Marburger⁽⁶⁾, respectively, in articles that are still frequently quoted. The theory indicates, and it is well borne out by experiment, that there is a distinct threshold power (not intensity) at which self-focusing occurs. Increase of power beyond the threshold leads to shortening of the focal length, and thus, by simple geometrical optics, to a variation in the amount of light passing through a remote aperture. Several devices using this phenomenon, or similar self-defocusing effects, to achieve power limiting of laser beams have been constructed, most notably at the Center for Research in Electro-Optics and Lasers, located at the University of Central Florida, Orlando, FL.^(7,8)

While these devices are too bulky for direct use in goggles or visors, they serve to demonstrate the basic feasibility of using self-focusing/defocusing phenomena for protection against laser threats. In lenslet arrays, the light beams incident on the nonlinear medium are strongly converging when they encounter the linear/nonlinear interface. While the basic self-focusing phenomena must be similar, detailed understanding of the nature of the beam propagation through the focal region and of the focal plane shifts that may be anticipated are subjects of current research throughout the world. It is not so evident that there should be a power threshold in small f /number systems; the phenomenon may be thought of more in terms of simple self-phase-modulation than in

terms of overcoming diffraction. Another obvious difference is that a spatially inhomogeneous beam is no longer required for self-focusing to occur; whatever the beam shape, the beam behavior in the focal region is likely to be extremely complicated.

To the extent that NLO material can be modeled as a thin lens, positive or negative, it is easy to calculate what it will have to do to meet the system requirements. For example, for a negative (defocusing) material, we have calculated that a change in focal length of $200\ \mu\text{m}$ in our representative system would produce a decrease of 10^4 in optical intensity reaching the retina. This is shown schematically in Figure 31.



- Modeling Nonlinear Optical Material as Thin Lens
- $200\ \mu\text{m}$ Shift in Focal Length \Rightarrow Optical Density of 4

Figure 31 Self-Focusing — Self-Defocusing

Other nonlinear phenomena, such as nonlinear absorption and scattering, have been suggested for protection of eyes and electronic sensors. In the case of nonlinear absorption, it should be remembered that by virtue of the Kramers-Kronig relations, there is a refractive effect associated with every absorptive effect; in the nonlinear regime, it is not always easy to separate them. The simplest absorptive effect, and the one most often suggested for protective applications, is saturable absorption. In a medium that shows this phenomenon, band-filling effects or other free-carrier-induced shifts of an absorption edge lead to light above a certain intensity level being absorbed very little. To use this phenomenon most effectively in a device, a catadioptric arrangement is necessary. While this has the great merit of redirecting the excess light out through the input aperture, obviating heat dissipation problems, it would be difficult to implement in the lenslet configuration.

Since the visible wavelength range covers a band less than 3 dB wide, two-photon absorption might be considered as a mechanism for broadband eye protection. Under conditions where simultaneous absorption of two photons through a virtual intermediate state can occur, the optical absorption may be written as

$$\alpha = \alpha_0 + \alpha_2 I,$$

where $\alpha_2 > 0$.

For a uniform beam of intensity I_0 incident on a sample of thickness L , the transmitted intensity is easily seen to be⁽⁹⁾

$$I = \frac{I_0 e^{-\alpha_0 L}}{1 + (\alpha_2 / \alpha_0) e^{-\alpha_0 L} (1 - e^{-\alpha_0 L})}$$

If $\alpha_0 L$ is not too large, the sample will transmit satisfactorily at low intensities, but as $\alpha_2 L I_0$ becomes large, the transmitted intensity will be reduced. The main difficulty with practical application of this mechanism is that the two-photon absorption coefficients α_2 are quite small. If we take $\alpha_2 = 10^4$ cm/GW, then for a 1-mm-thick sample we do not attain a 40 dB reduction in input intensity until the input intensity I_0 reaches 10 GW/cm². Even if the focal spot size were as small as 10 μ m diameter, we would still need 10 kW incident on a lenslet to achieve the desired effect. It should be noted that 10⁴ cm/GW is a very large nonlinear absorption coefficient⁽¹⁰⁾, observed to our knowledge only for narrow-gap semiconductors in the infrared, and considerably greater than any value found in the visible. There does seem to be some possibility of utilizing two-photon absorption in combination with other phenomena.

So-called reverse saturable absorbers, such as indanthrone and its derivatives, have been investigated recently⁽¹¹⁾. In these materials, electrons excited by absorption of photons are transferred to a long-lived excited state with a much higher absorption cross section. Such materials are capable in principle of providing broadband protection. The present materials require high intensities (in the range of 1 TW/cm²) to afford effective protection and are absorptive at low light intensities.

In order to estimate the NLO material requirements, a system, originally analyzed by Hermann⁽¹²⁾, was investigated and showed that, for a nonlinear refractive medium of good transparency, with a Gaussian beam roughly comparable to the lens diameter impinging on it, effective limiting would require

$$n_2 I_0 \geq (2\lambda^3 F^2) / (\pi^3 w_0^2 L),$$

where, n_2 is the nonlinear refractive index, I_0 the peak on-axis beam intensity, λ the free-space wavelength, F the lenslet f/number, w_0 the Gaussian beam radius, and L the nonlinear material thickness. Effective optical limiting was assumed to occur when a phase shift of 180 degrees occurred in the optical beam. Such rules of thumb are invaluable in determining whether a given lens-design/nonlinear material combination is capable of providing an effective response to a potential threat.

As an example, consider a lenslet array, similar to those currently being analyzed, with the following parameters:

$$\begin{aligned} \lambda &= 0.5 \mu\text{m} \\ F &= 1.8 \\ w_0 &= 500 \mu\text{m} \\ L &= 25 \mu\text{m} \text{ (conservative value).} \end{aligned}$$

L might be the actual material thickness or, more likely, it might be the effective thickness where the near-axis beam intensity is close to its maximum value. Calculations indicate that this effective thickness may be quite small, perhaps as little as 25 μm for the lenslet array. As a conservative estimate, we adopt this value. Then, with the other quantities as given above, we need $n_2 I_0 \geq 4 \times 10^9$ for effective limiting. There appear to be reasonably fast, broadband organic materials with nonresonant n_2 at least as large as $10^{-6} \text{ cm}^2/\text{MW}$; they would provide limiting for a beam with $I_0 > 4 \times 10^3 \text{ MW/cm}^2$, or in other words, for a beam of something under 40 W total power incident on one lenslet. This is above the minimum eye-damage level around 1 W/mm², but it

is sufficiently close that an optimized system design and modest material improvements would make a useful system.

Figure 32 shows a summary of some of the optical limiting and switching concepts that have been proposed over the years⁽⁹⁾. Some of these may be applicable to the lenslet array concept but further analysis is required.

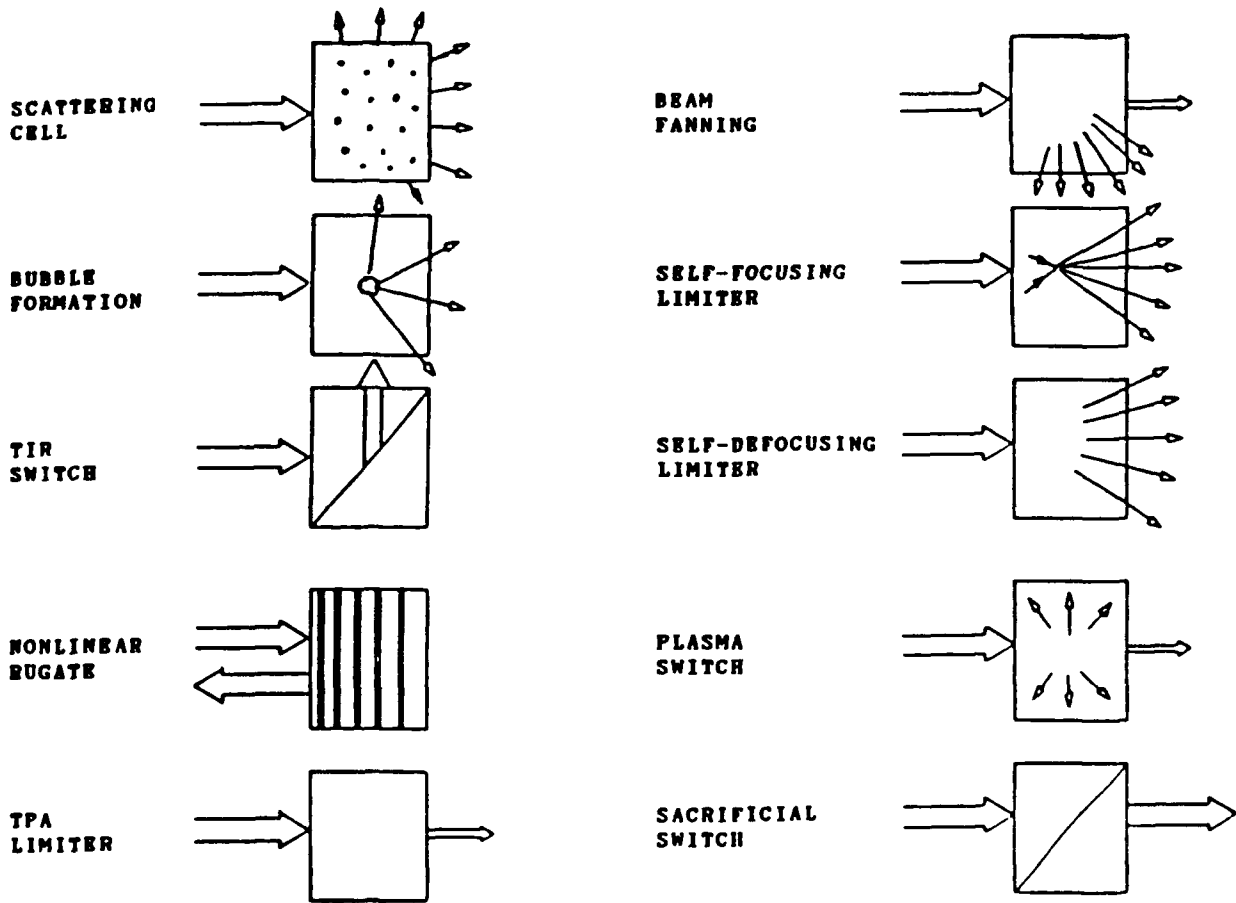


Figure 32 Various Proposed Optical Limiting and Switching Concepts

5.0 PHASE III EFFORTS

5.1 Lenslet Eyepiece, Goggle Design and Fabrication

To overcome the limited FOV of each lenslet element, the eye-protection device was configured such that the lenslet elements fanned radially outward from the center of the iris of the eye so that the optic axis of each of the individual lenslet quads crossed the optic axis of the eye at the center of the iris (the pupil). This curvature determines the goggle's FOV. The wide FOV of the eye is due to the fact that light incident at different angles is accepted by the eye if the light passes through the iris without being absorbed by the pupil. Extending this idea to the goggle system suggests that light which passes through the lenslet elements and also passes through the pupil will contribute to the overall FOV of the goggles.

To verify this, rays were traced from a distant object encompassing a FOV of 137 degrees. The rays were incident on the eye, with no intervening goggles and focused on the retina as expected as shown in Figure 33. Next, the modeling was repeated; however, this time the modeling included an array of lenslet elements in front of the eye. Figure 34 shows the bundles of parallel light rays traced through the lenslet elements and emerging to pass through the center of the iris, and finally focusing on the retina. All rays contributed to the goggle's FOV and showed the same results as without goggles.

Because of the orbital motion of the eye, centering the curvature of the goggles on the center of the eye's rotation also produces a viable design. These results are shown in Figure 35. In this case, only the light passing through about three adjacent lenses passes through the pupil and is focused onto the retina. The rays passing through other lenses are intercepted by the other parts of the eye and are not allowed to enter the pupil. As the eye moves, the rays from these other lenses will be allowed to pass through the pupil.

A subtle simplification used during the discussion of Figures 33 and 34 was that parallel light rays were assumed to be incident on the eye. Such an approximation is valid to a large extent, especially for distant objects. However, the concern was whether or not a real object, at a finite distance from the observer, could be imaged onto the retina of the eye. To understand this more clearly, an analysis was performed as indicated in Figure 36. The analysis was as follows: consider an object, such as a tree, 10 m away from the observer wearing the goggles. The FOV of the goggles and the eye are such that the entire tree can be seen without moving the eye. Light rays pass through the curved goggles and form an image on the retina of the eye. Light scattered from a point, on the base of the tree, in line with the optic axis of the eye, passes through the central lenslets and is

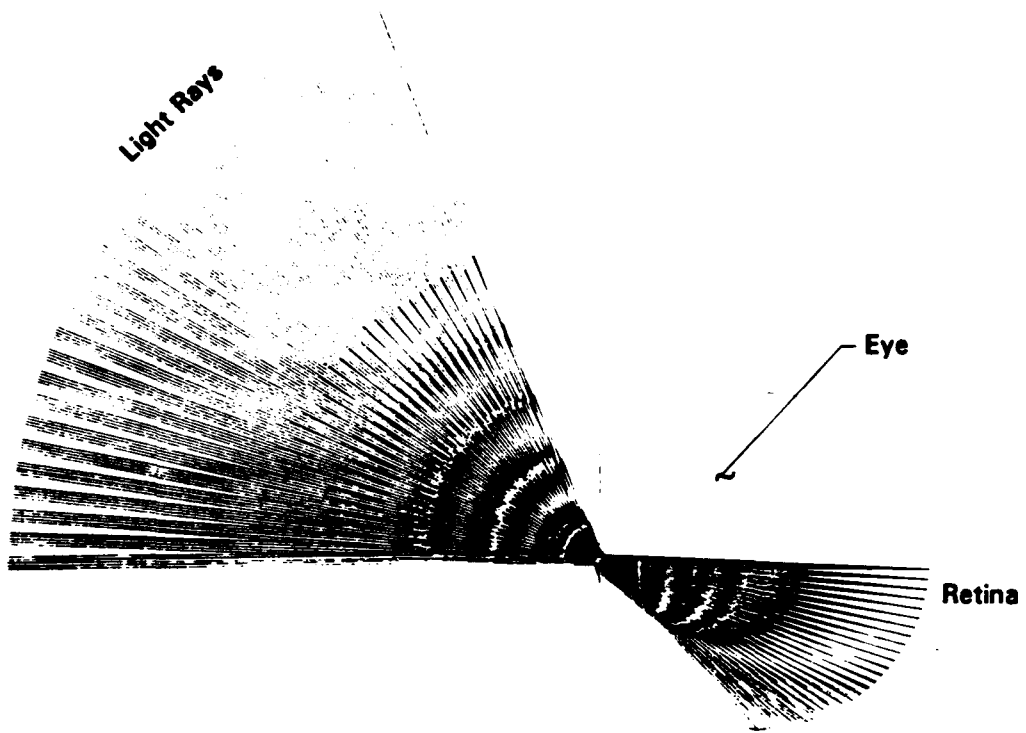


Figure 33 Light Rays Incident on the Pupil Focus on the Retina

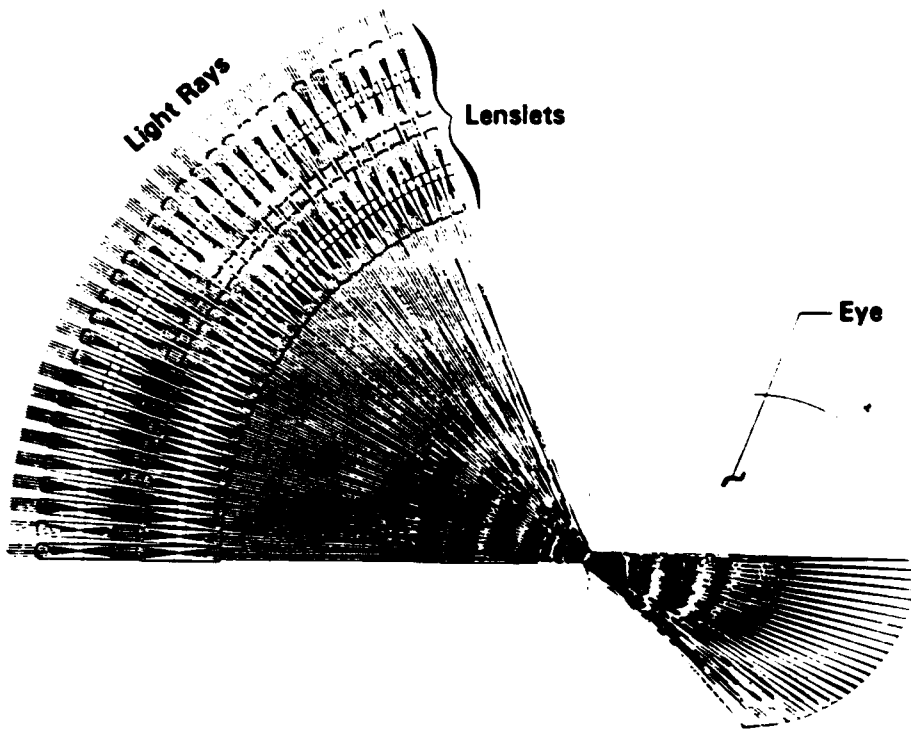


Figure 34 Radial Placement of Lenslets in the Goggles Results in a Wide Field of View

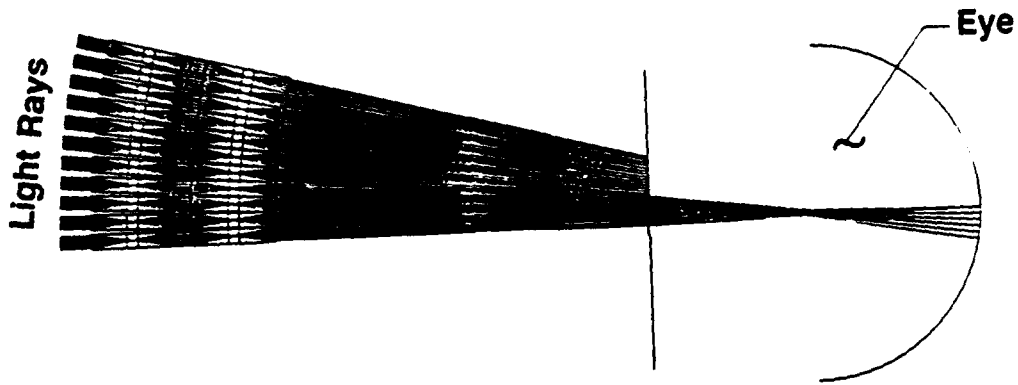


Figure 35 Goggle Design Centered on Eye's Center of Rotation

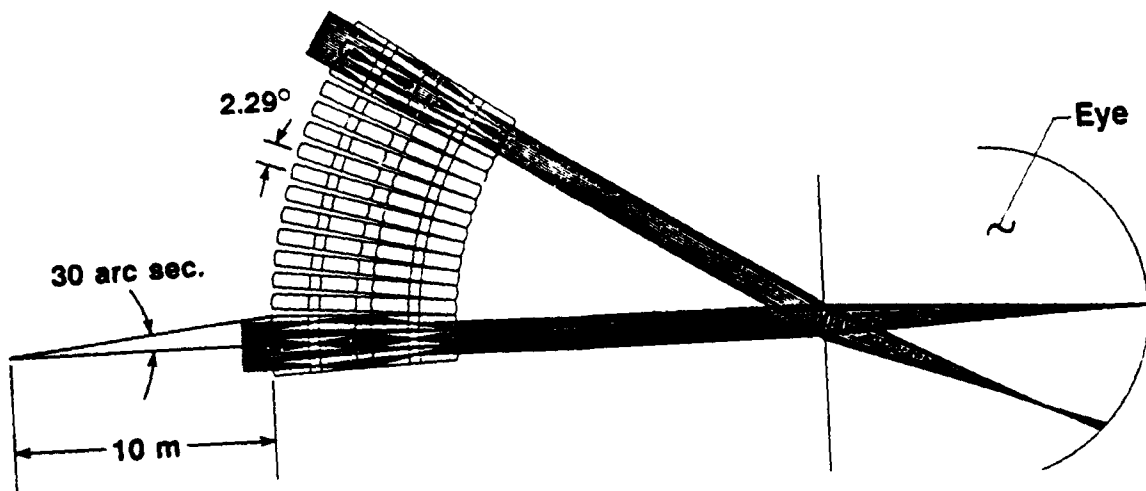
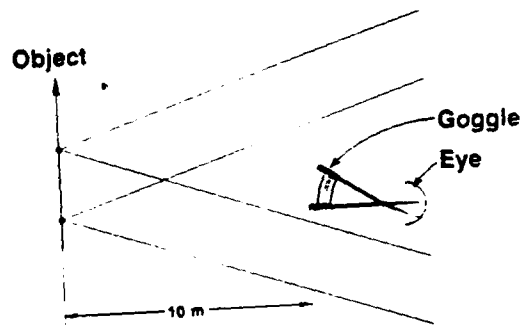


Figure 36 Image Transfer of an Object 10 m Away from the Observer

imaged on the center of the retina. Only the light rays which fall into a narrow cone of roughly 30 arc seconds will be transmitted to the retina of the eye and, as the figure shows, imaged to a point. Therefore, a point in the object plane (tree) is focused to a point in the image plane (retina). This is an important requirement for image transference. Angles greater than 30 arc seconds will be stopped by the entrance pupil of the eye. Of course, the image is composed of many point sources on the object, at different spatial locations, and these point sources will be transmitted through the various lenslet elements creating the overall image on the retina of the eye. Therefore, light scattered from a point high on the object passes through the goggle elements at a position above the eye's optic axis, and forms an image on the retina below the on-axis point. Thus, an inverted extended image is formed on the retina. Notice that the point focussed to the lower region of the retina is not a point but rather a slightly misfocused spot. This is due to spherical aberrations of the eye and not to any inadequacy of the lenslet design.

In a final design, centering the lenslets on the center of rotation of the eye and allowing the individual lenslet quads to have a FOV of 10 - 15 degrees will be required to provide both peripheral vision and allow for nominal eye motion. Investigation into the sensitivity of precisely locating the goggles with respect to the eye must still be evaluated but is not believed to be a significant issue.

An algorithm was developed to determine the precise position of each tube in a closely packed configuration. Using the diameter of a given lens at a desired radial distance, the program calculated the number and angular position parameters of tubes which would fit a hemispherical surface. This information was subsequently used by a numerically controlled five-axis miller to accurately bore holes into an aluminum dome.

Since the eye has close to diffraction-limited performance for apertures between 2-3 mm, the back aperture of the lenslet quad was made of similar dimension. The minimum distance from the cornea to the back surface of the eyepiece was estimated to be 10-15 mm, depending on the length of an individual's eyelashes. Using 17 mm as a comfortable relief distance and 2 mm as a back aperture diameter, a 3.3 degree taper half-angle was calculated for the conical tubes. The use of conical tubes is discussed in Section 5.2. A 3 degree half angle tapered end mill was readily available and was used. The aluminum eyepieces were machined and anodized and consisted of 4 mm entrance apertures and 2 mm exit apertures.

A front view of eyepiece is shown in Figure 37. The eyepiece has a radius of curvature of 36 mm with a radial thickness of 20 mm. Two hundred and fifteen holes were machined into the aluminum eyepiece, using a numerically controlled miller, to allow for eventual insertion of the lenslet quads.



Figure 37 Front View of Lenslet Eyepiece

Shown in Figure 38 is the visual performance of the eyepiece without any lenslet elements. As can be seen, there is no noticeable degradation in the FOV of the eye by using the eyepiece. This indicates that the eyepiece concept and preliminary design are viable for holding the lenslet elements.

In order to provide a better visual performance assessment of the eyepiece concept, two eyepieces were incorporated into the standard Army issue Sun, Wind, and Dust goggle frame as shown in Figure 39. Rudimentary visual performance tests were performed by Battelle staff by allowing them to wear the goggle device and walk the corridors of Battelle or allowing them to perform some function outside. Peripheral vision was quite good; however, due to the current design limitations, any orbital motion of the eye quickly produced an obscuration of the visual field. Staff commented that training one's self not to move the eye but rather to move the head in the direction one wanted to look was unusual but that possibly they could get used to it. In any event, they could still perform the specific tasks required of them when wearing the goggles. It is anticipated that a future design will overcome the current restriction on the orbital motion of the eye introduced by the eyepiece.

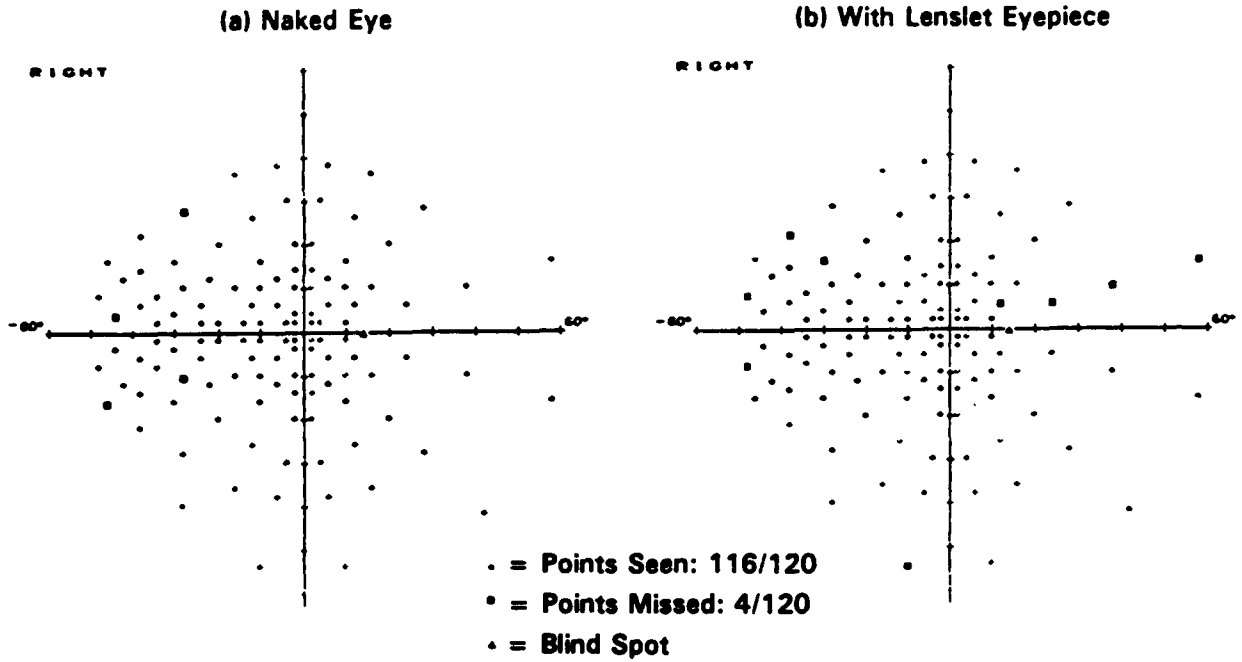


Figure 38 Humphrey Field Analyzer Visual Performance Tests
 (a) Human eye performance without eyepiece,
 (b) Human eye performance while looking through
 eyepiece without lenslet elements

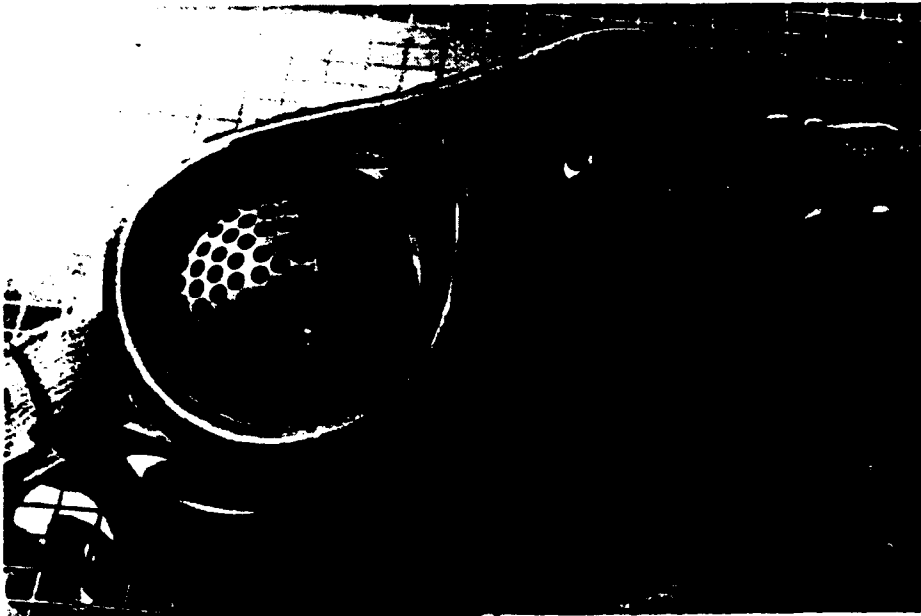


Figure 39 Laser Eye Protection Goggles

5.2 Conical Quad Design

Due to the limited FOV provided by each lenslet quad and, by contrast, the large FOV provided by the human eye, curving the surface of the lenslet array into a hemispherical surface overcame many of the limitations of a flat panel lenslet array. A refinement to this originally proposed hemispherical eyepiece is discussed here.

Phases I and II assumed that the assembled lenslet quads would consist of an array of cylindrical tubes that would be machined into a hemispherical eyepiece. Because of the radial thickness of the eyepiece, significant regions would exist at the outer surface of the eyepiece where no refractive surface (lens) was present even though the tubes would be closely packed at the inner surface of the eyepiece. This noncomplete packing at the outer surface of the eyepiece was alleviated by making the diameter of the outer lens proportional to the radius of curvature of the eyepiece's outer surface. This in turn made the tubes conical instead of cylindrical. The advantage of this approach is that it allows a wider FOV for the eye through each tube by virtue of the nonzero taper angle of the wall. For example, a 20 mm length cylindrical tube with 2 mm entrance and exit apertures provides a maximum FOV of 5.7 degrees. In contrast, a conical tube of the same length but with entrance and exit apertures of 4 mm and 2 mm, respectively, provides a maximum FOV of 8.5 degrees. This represents an increased FOV of 50% by using a conical design.

Figure 40 shows a preliminary design for the conical lenslet quad design. The first lens is 4 mm in diameter while the fourth lens is 2 mm in diameter. The overall length of the quad unit is 20 mm. Spacers are also shown as a technique to locate and center the four lenslet elements precisely. A detailed evaluation of the optical performance characteristics of this design, referred to as PROTO90Q, is presented in Section 5.3, while the fabrication effort is presented in Section 5.4.

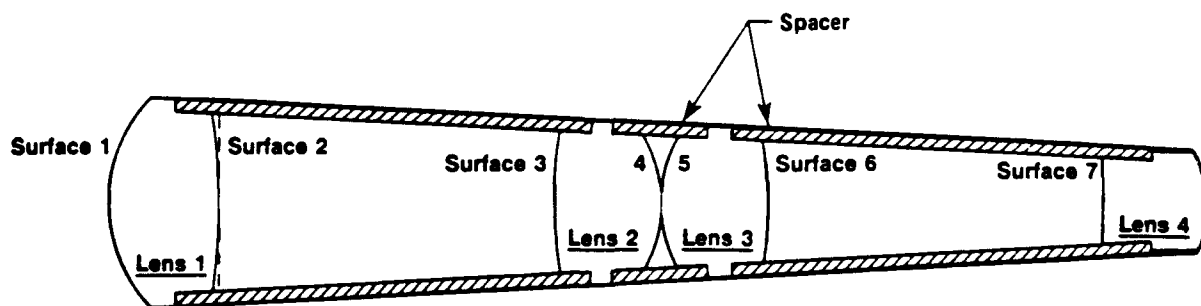


Figure 40 Conical Lenslet Quad Design

5.3 Baseline Lenslet Design Performance Characteristics - PROTO90Q

As part of the Phase III effort, a detailed lenslet design was developed based on the best understanding of the optical performance required as well as available fabrication techniques. As indicated within this report, many factors are involved in developing a viable lenslet design. In an attempt to minimize costs, but still gain a significantly better understanding of the design process, the PROTO90Q design was developed for eventual fabrication. PROTO90Q focusses on two primary factors in developing a viable design. First, a diffraction limited spot size produced by the first lenslet to eventually be used by the NLO material. Second, maximum FOV while retaining good visual performance.

These lenslets are designed to provide reasonable visual acuity and FOV for the eye. They are designed to demonstrate initial feasibility and manufacturability using a plastic lens molding technology. They are not however, designed to address all the difficult issues associated with the proposed application. Specifically, they do not adequately allow for normal eye motion. When one looks off to the side, by moving their eye, significant vignetting occurs. This current lenslet array is also designed to function optimally only at one wavelength; it is not chromatically corrected over the entire visible region. This was intentional because chromatic correction requires an achromatic lens structure incorporating either additional refractive elements or the possible use of diffractive optics. This added complexity was not warranted for the first generation design. Also, this first design did not incorporate the NLO limiting material so vital to the ultimate application of this device. These as well as other factors will certainly need to be addressed to produce a viable lenslet design, but for an initial fabrication effort these factors were considered beyond the scope of this current effort.

The following six figures summarize the optical performance of the lenslet array designed under this phase. The design was designated PROTO90Q and was optimized for best visual performance at 2.25 degrees off-axis at a wavelength of 587 nm. The 2.25 degree off-axis optimization criterion was used to maximize the useful FOV of the lenslet quad.

Figure 41 shows the optical system layout with a schematically modeled human eye. The incident collimated light is focused at two positions in the quad telescope. The front 4 mm diameter lens is optimized to collect and focus the incident radiation to a diffraction limited spot on-axis. This first focal point provides a location where NLO material can eventually be incorporated. The following three lenses reinvert the image and recollimate the light. Finally, the light enters the eye and is focused at the retina.

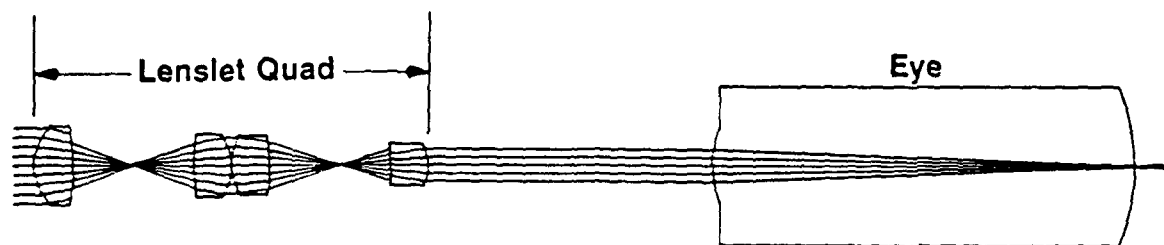
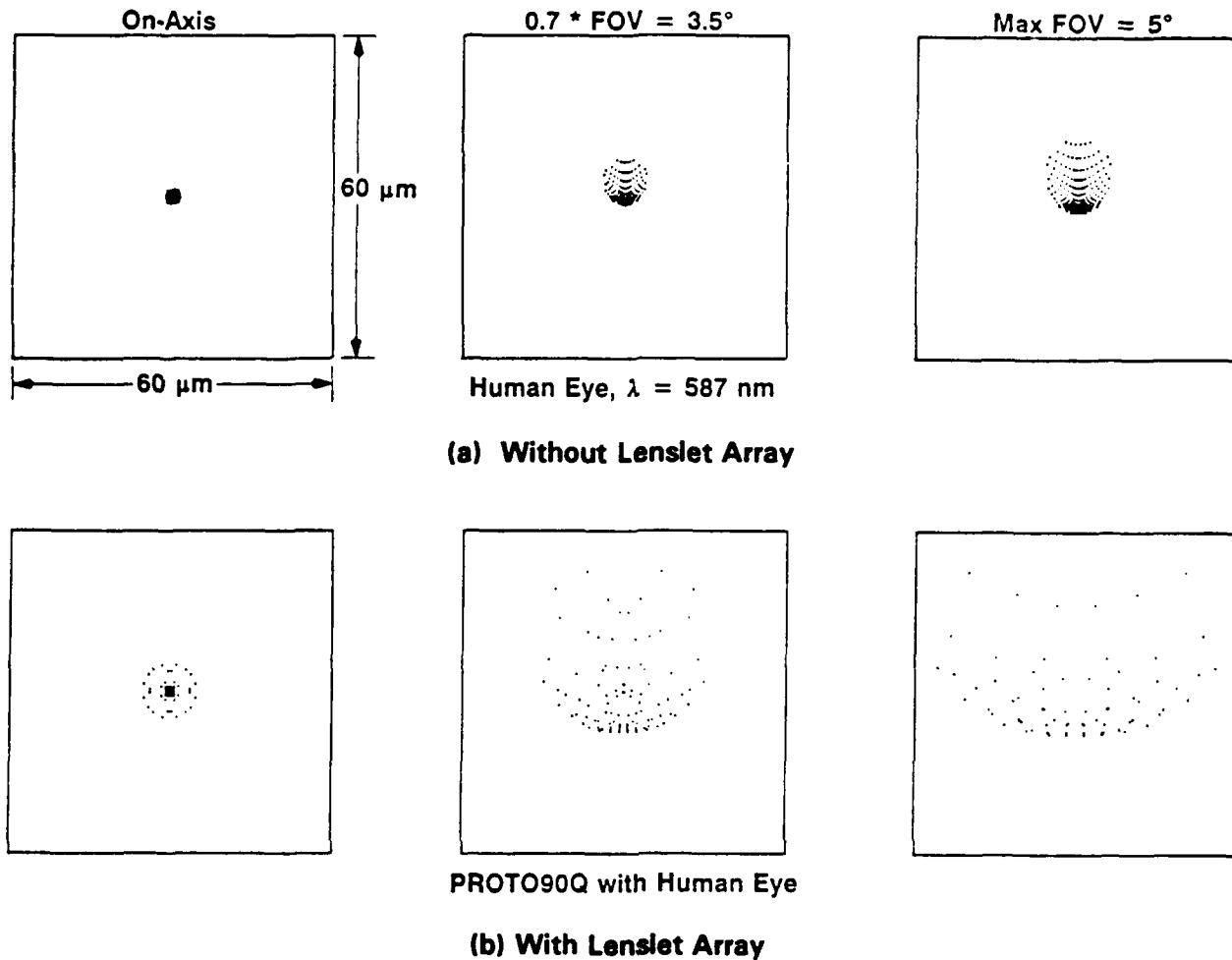


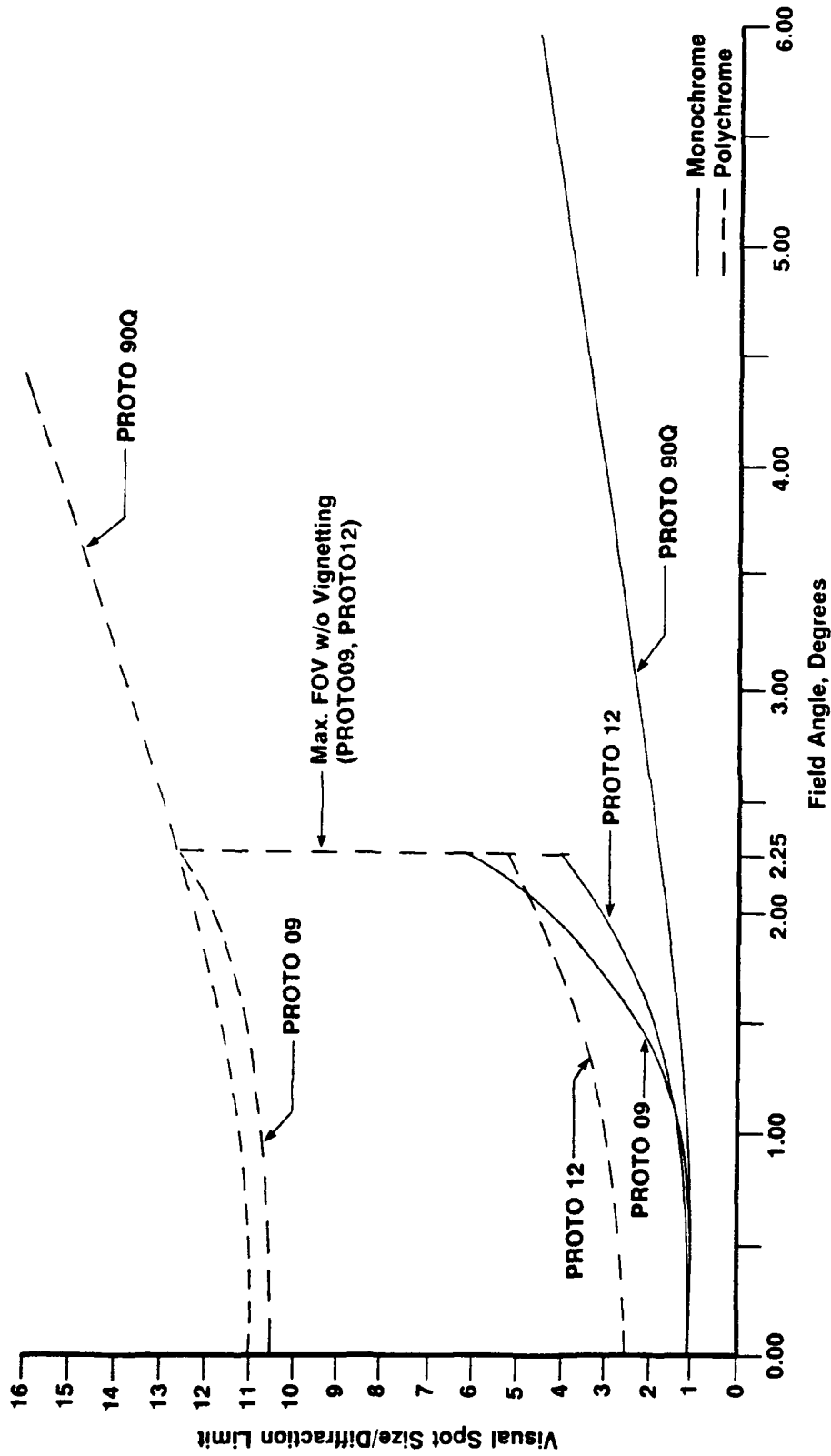
Figure 41 Optical System Layout PROTO90Q

Figure 42 shows the effect of placing the lenslet array in front of the eye. These spot diagrams represent the image pattern expected on the retina of the eye for collimated light incident on the eye at various angles of incidence. Figure 42a shows the spot diagrams for the human eye alone, without the lenslet array; while Figure 42b shows the effect of placing the optical device in front of the human eye. Three field angles (0, 3.5, 5 degrees) were evaluated to show the degradation of the spot off-axis. The scale width of the boxes is the same in all six cases at $60 \mu\text{m}$ on a side. The eye performance naturally degrades off-axis away from the fovea as shown in Figure 42a. The relative increase in the degradation due to the use of the PROTO90Q quad can be seen by comparing the two plots. On-axis, there is negligible degradation and the effect on a person wearing such a device would probably be tolerable and acceptable. Off-axis, there is significant distortion and the perceived effect on an individual remains to be determined. Since most of the time, when good vision is required, a person will utilize the foveal part of the eye, or high acuity region, and use the peripheral vision only to detect motion, this degradation may not be as important as it may seem.



**Figure 42 Comparison of Spot Diagrams
(a) Without and (b) With Lenslet Array**

Figure 43 shows a comparison between the expected spot size on the retina for the PROTO90Q design and for previous designs, as a function of field angle. Notice that the PROTO90Q design provides the best performance as a function of field angle. Both monochromatic and polychromatic data are shown; however, no chromatic correction was provided for in the design. This would have required achromat lenses and was beyond the scope of the current effort. The PROTO90Q design allows near diffraction limited performance out to almost 3 degrees.



Diffraction limit of 2 mm dia. aperture at $\lambda = 0.588 \mu\text{m}$.
 Total quad length = 25.12 mm (PROTO09, PROTO12).
 Total quad length = 20.00 mm (PROTO90Q)

Figure 43 Visual Spot Size for Conical Quad Aspheres

The overall effect and interrelationship of field angle, visual acuity, contrast, chromaticity, peripheral vision, and vignetting must still be determined in order to produce a completely acceptable design for a frequency agile eye protection device. PROTO90Q represents a first step in that direction.

Figures 44a and 44b show the on-axis and off-axis wavefront error of the lenslet quad. The horizontal axis represents 2 mm, the width of the exit aperture of the fourth lens. The on-axis performance is better than tenth-wave. Off-axis, at 0.5 degrees, the wavefront error is approximately quarter-wave.

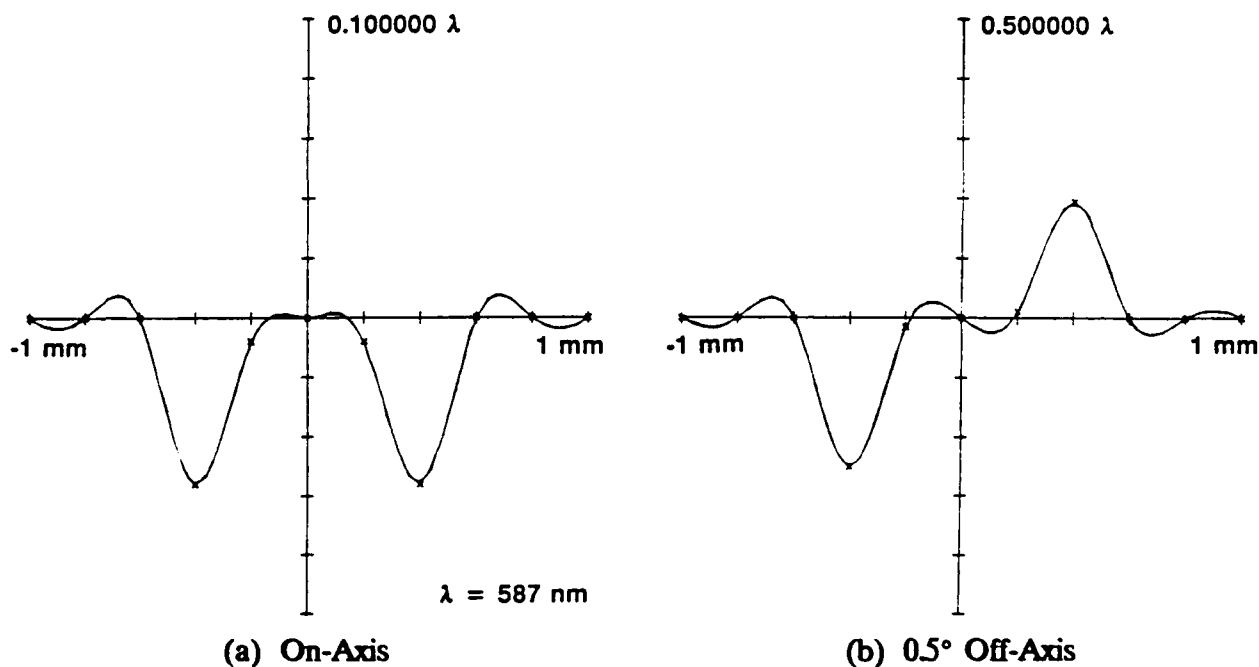


Figure 44 Wavefront Error for PROTO90Q Quad

The effect of vignetting on light transmission through the PROTO90Q design was also investigated. Figure 45 shows this effect as a function of field angle. For a half-angle field of view of up to 4 degrees, very slight vignetting occurs; however, for larger field angles, the amount of light transmission is reduced. This is in addition to the reduced visual acuity produced by the lenslet design as a function of field angle; that is, the amount of light that gets through the system is also reduced. As was indicated in Section 5.2, a useful quad field angle on the order of 12 degrees will be required to allow simultaneously good peripheral vision and orbital motion of the eye. However, as shown in Figure 45, the light transmission goes to zero at 12 degrees. This observation shows again that further effort is required in the design of the optics and array to balance all of the performance parameters. It does not necessarily demonstrate a fundamental limitation of the eye protection concept.

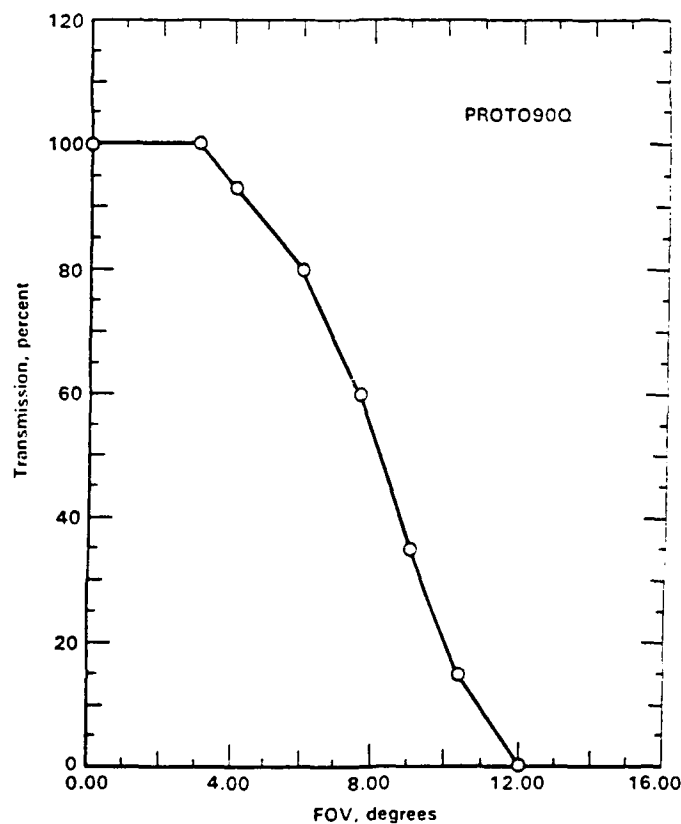


Figure 45 Percent Light Transmission of Lenslet Quad

Figure 46 shows a comparison, in terms of MTF, of the PROTO90Q design, the commercially available design by Aeroflex, and the unaided eye. The PROTO90Q design represents a significant improvement over Aeroflex's original design. Also, the lenslet made by Aeroflex Laboratories, Inc., may be considered comparable to the spherical micro-integrated lenses (SMILE™) available from Corning. It should also be noted that the design by Aeroflex represents only two planes of lenses as opposed to the four used in the PROTO90Q quad design. In other words, the design by Aeroflex, as shown, produces an inverted image; two additional planes of lenslet elements would be required to match the PROTO90Q design. This would degrade the performance of the lenslets available from Aeroflex even below the level shown.

At low spatial frequencies the PROTO90Q design exceeds that of the human eye; while, at higher frequencies it performs slightly worse. Low spatial frequencies allow recognition of objects; while, the higher spatial frequencies provide the contrast and detail of an object. Further effort is required to increase the higher frequency component of the current lenslet design.

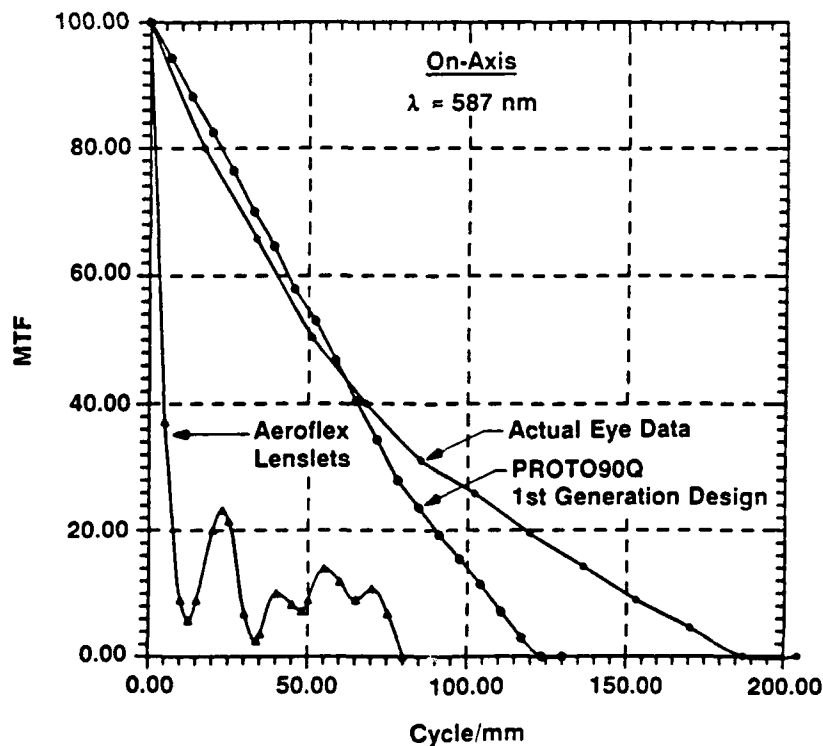


Figure 46 Performance Comparison of Various Lenslet Systems

Finally, Figure 47 shows the roll-off in optical gain at the first focal point as a function of incident angle. On-axis, the gain is in excess of 10^6 , but rapidly falls off as the incident angle is increased. The middle curve shows 100% of the encircled energy (ENC), while the top curve shows 80%. In essence, this says that 80% of the energy has a gain in excess of 2×10^5 at an incident angle of 3 degrees. For example, if a NLO material had optical-limiting capability for gains in excess of 2×10^5 then 80% of the energy would be blocked if the incident angle was 3 degrees. This also says that 20% of the energy would get through the lenslet array. The effect of off-axis rays on optical limiting must be further addressed under a future program.

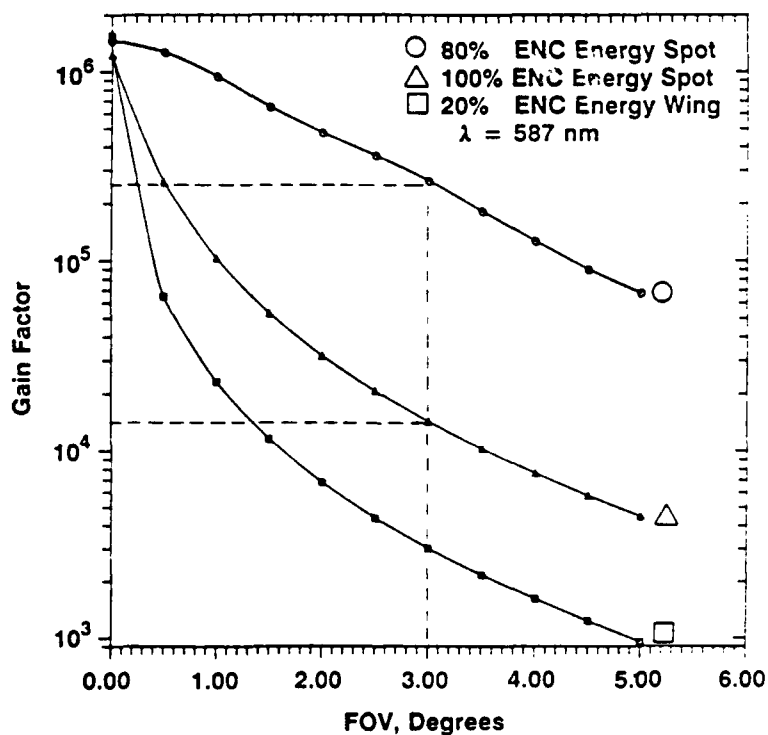


Figure 47 Gain Degradation as Function of Incident Angle for First Lenslet Element - PROTO90Q

5.4 Initiation of Subcontract to Mold Custom Lenslet Design

Fabrication of the lenslet elements took place as subcontracted items outside of Battelle. Several plastic molding companies were contacted to see if they could meet the high precision tolerances required for the lenslet elements. A number of vendors were very expensive or were not capable of meeting the required specifications. Plastec, Inc., of San Dimas, California, was then contacted. After several phone conversations concerning the fabrication process a subcontract was initiated. A phased program was established with four milestones to minimize risk. These milestones are indicated below:

(1) Review of Engineering Design

After Battelle review, FAX sent from Battelle to signify approval for continuation of purchase order.

(2) Metal Pin Insertion Inspection

(a) A third party, independent inspection will be performed by Laser Power Optics to quality surface figure of pins.

(b) A third party, independent inspection will be performed by Dimensional Inspection Laboratories to mechanically inspect pins for tolerance.

After Battelle review, FAX sent from Battelle to signify approval for continuation of purchase order.

(3) Fit, Form, and Function

Fit: verify assembly will fit together,

Form: verify assembly will fit holder matrix provided,

Function: verify optical performance

After Battelle review, FAX sent from Battelle to signify approval for continuation of purchase order.

(4) Molding Run of 200 Pieces

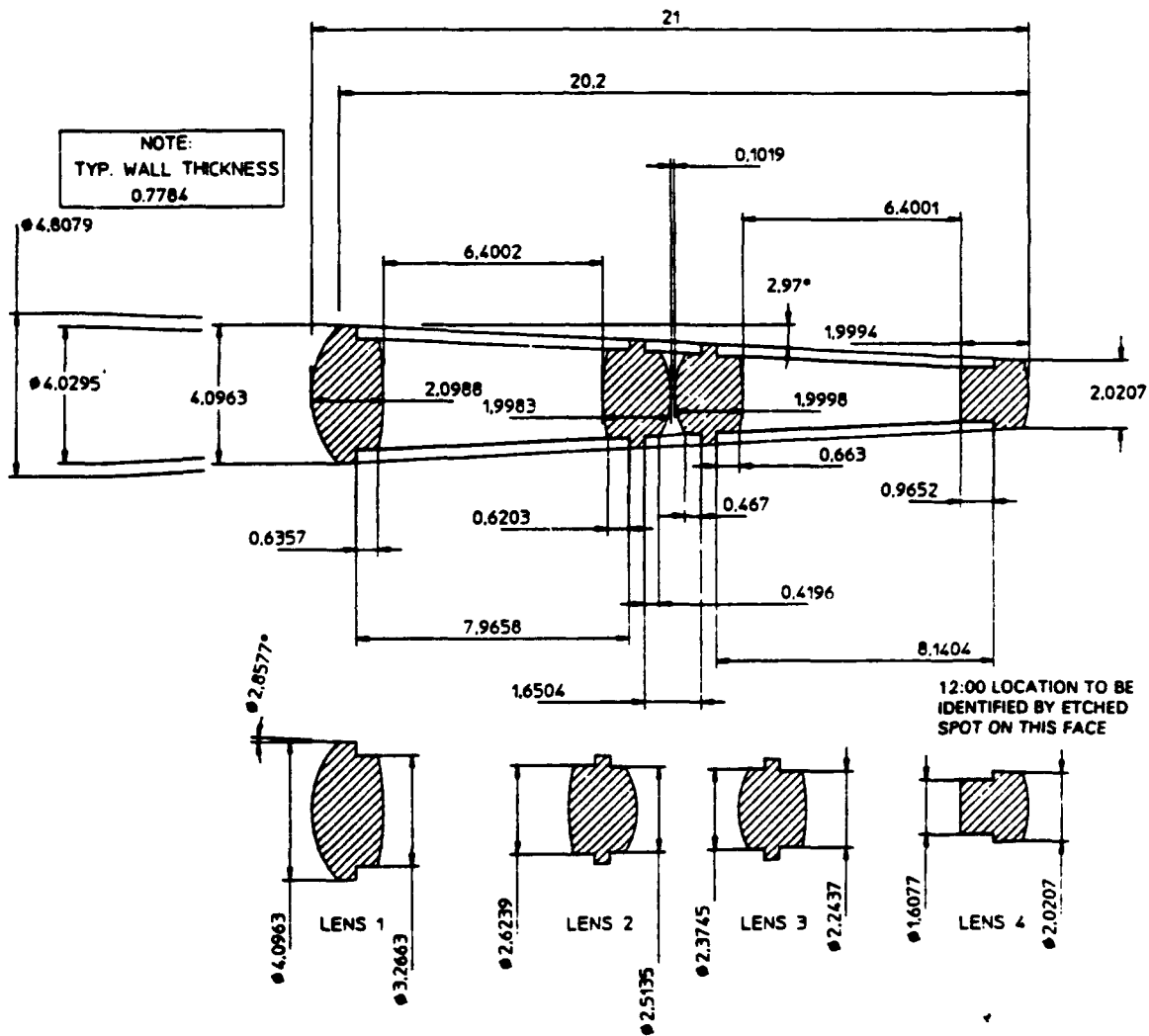
After Battelle review and inspection of final pieces, final payment sent. Battelle holds the right to make one on-site visit to Plastec, Inc. to verify performance quality.

Under the first phase, Plastec, Inc., developed a tooling blueprint using the PROTO90Q lenslet design. This design included precision spacers to hold the lenses at the appropriate distances in the conical tubes. Plastec's approach was to mold all four lenses simultaneously in one mold in an effort to keep the costs low. Figures 48 and 49 show the engineering blueprint and the configuration of the mold, respectively.

After several blueprint iterations, authorization was given by Battelle to Plastec, Inc., to proceed to the next phase. The tooling was prepared by Plastec, Inc., and the optical surface quality of the molding pins as well as the mechanical tolerances were inspected by a third party. Following this inspection authorization was given to proceed to the third phase. After some initial errors in the cutting of the precision pins which mold the surfaces of the lenses, Plastec, Inc., began to send samples of the molded parts. At first the lenses were not completely filled out. Parameters of the injection molding process, such as pressure, temperature, and venting of vaporized gases, were still being optimized. Samples were received from Plastec, Inc., on a weekly basis during February and March 1991. Each new set of molded optical parts showed a small improvement in the packing of the polymethyl methacrylate (PMMA) into the mold and also in the clarity of the plastic itself. Evaluation of these delivered lenslets took place in Phase IV.

KEY	DESCRIPTION	APPRVD DATE
A	ADD ID. TO LENSES	10-30-90
B	ADD KNUBBIN OPTION	10-30-90


ACTUAL SIZE



TELE. NO. (714) 592-8333				SEE DRWG	
FAX. NO. (714) 592-8843		MATERIAL DESCRIPTION		MATL SPEC	
DO NOT SCALE THIS DRAWING	DRAWN BY D. RICHARD	DATE	BATTELLE LENSLET ASSY		PLASTEC, INC.
DIMENSIONS: X 15	DESIGNER	10-18-90	TITLE		451 COVINA BLVD.
XX 1	RELEASED BY		NEXT ASSEMBLY		SAN DIMAS, CA.
XXX 2	SUPERSEDES DWG.		FINISH	SCALE 10X	PART NUMBER

Figure 48 Engineering Drawing of Lenslet Quad Produced by Plastec, Inc.

6.0 PHASE IV EFFORTS

6.1 Experimental Evaluation of Custom Molded Lenslets

Various techniques were used to evaluate the lenslets received from Plastec, Inc., as well as from other commercial sources. In the first series of experiments, the Plastec lenslets were placed on a 20 lp/mm Ronchi grating and imaged onto a Cohu charge-coupled-device (CCD) camera. The output of the camera was digitized by a computer and displayed on a TV monitor. A light table underneath the set-up provided a diffuse ambient background illumination. The fringes cast by the ruling were then used to diagnose the overall quality of the lenses. During the molding process, nonuniform cooling of the PMMA polymer caused strains in the material. These strains or refractive index inhomogeneities produced severe slope changes or distortions in the image of the Ronchi fringes. Polaroid photos were taken of each lens' fringe pattern. A qualitative ranking was made based on this visual record. Photographs of the images produced on the TV monitor by representative lenslet samples, for each of the four lenslet designs required to produce a quad, are shown in Figures 50a through 50d. The distortions produced by these lenslets are clearly visible. The lenses adjudged best, by examination of these test patterns, were used in subsequent characterizations.

In the second series of experiments, the focal region of the first lens was evaluated for minimum spot size. The data collection technique again used a CCD camera, computer, digitizer, and TV monitor. Figures 51a through 51c show the focal region as seen by the camera. Figure 51b represents the best focus, while Figures 51a and 51c show the beam quality approximately 200 μm on either side of best focus. For these, and subsequent experiments, a multiwavelength He-Ne laser was used. The output wavelength of the laser was 594.1 nm; very near the lenslet design wavelength of 587.6 nm. The spot size at best focus was greater than 50 μm in diameter. This is in contrast to the expected near-diffraction-limited performance of 3 μm for this lens. Also, one can see significant asymmetry of the beam as it passes through the focal region. The image 200 μm before best focus shows a racquet-like pattern. The "handle" of this image is oriented at the position of the sprue in the mold master. (The sprue is the channel through which the hot plastic flows into the lens region.) Apparently, during the molding process, the temperature differential along this region led to some strain in the material and this, in turn, affected the lens' performance. Distortions were produced on the surface of the lens as well as internally.

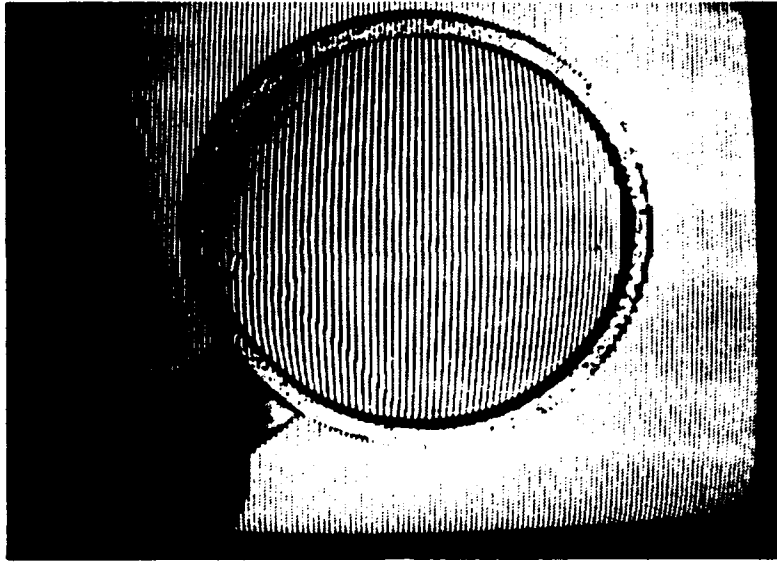


Figure 50a Representative Sample of the Optical Quality of the Fabricated Lens 1 Design Received from Plastec, Inc.

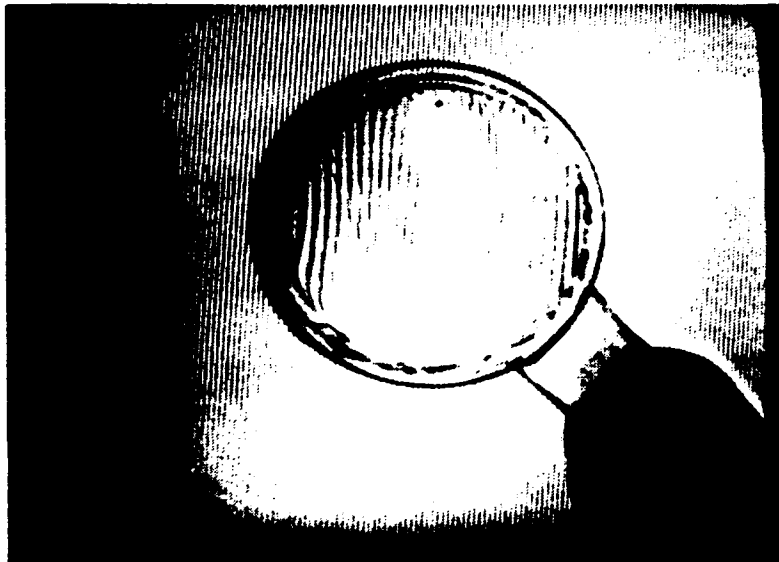


Figure 50b Representative Sample of the Optical Quality of the Fabricated Lens 2 Design Received from Plastec, Inc.

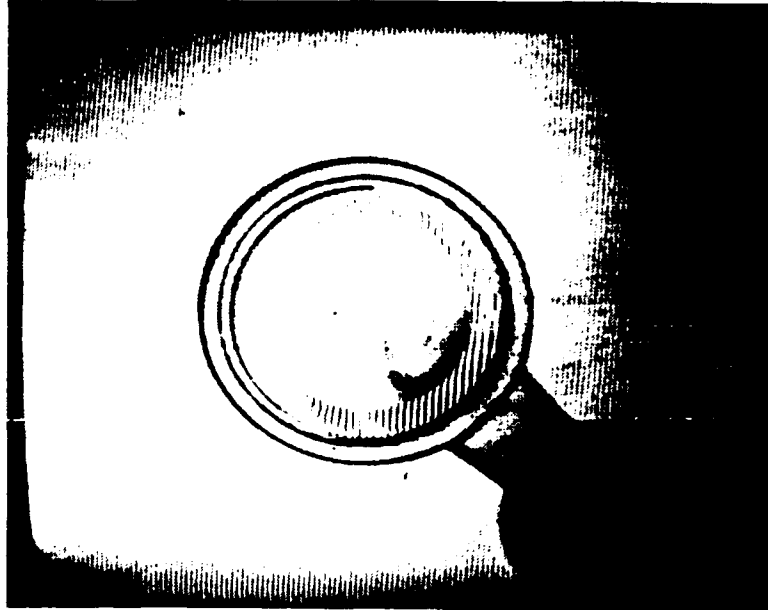


Figure 50c Representative Sample of the Optical Quality of the Fabricated Lens 3 Design Received from Plastec, Inc.

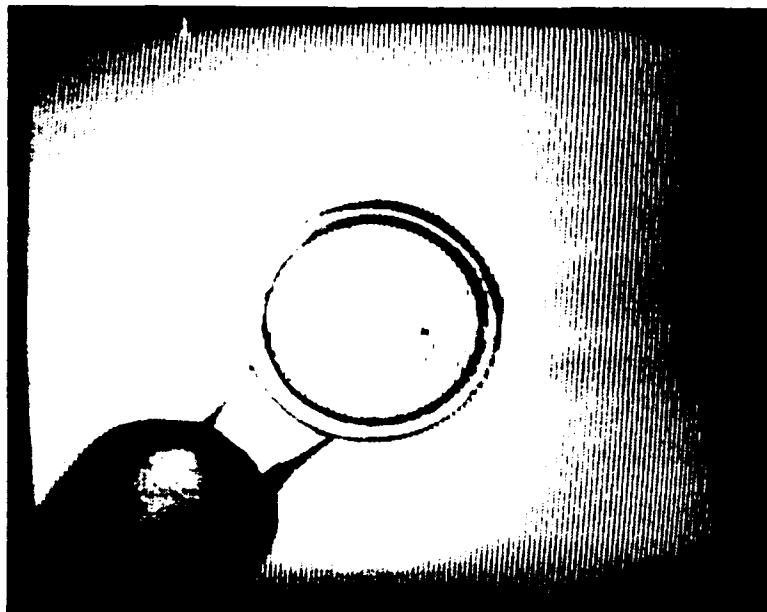


Figure 50d Representative Sample of the Optical Quality of the Fabricated Lens 4 Design Received from Plastec, Inc.

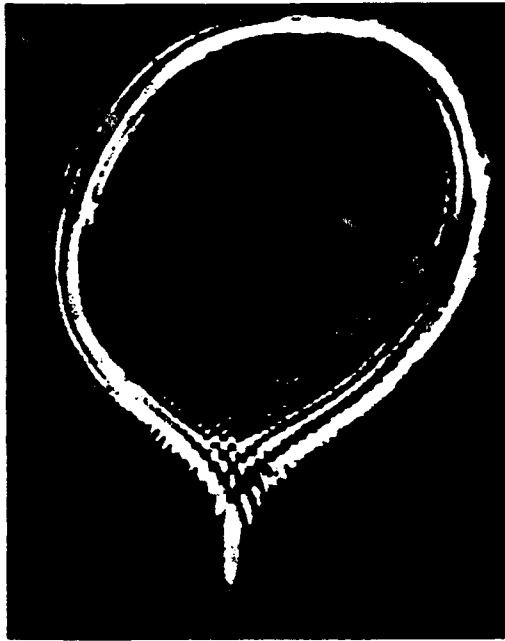


Figure 51a
Spot Size of Lens 1 as Seen by
CCD Camera 200 μm in Front of
Best Focus



Figure 51b
Spot Size of Lens 1 as Seen by
CCD Camera at Best Focus



Figure 51c
Spot Size of Lens 1 as Seen by
CCD Camera 200 μm Behind
Best Focus

In addition to spot size, the focal position relative to the back surface was measured. The paraxial focus was measured to be 238 μm beyond the design focal position. The smallest spot diameter with full aperture ("best focus") was measured to be 60 μm inside of the intended design focal position. Thus, the spherical aberration of the system was on the order of 300 μm . The design of PROTO90Q called for this to be 7 μm . Obviously, the fabrication was significantly inaccurate. To evaluate this further, the actual shape of the front surface of the lens was measured. By looking at the lens from the side (edge-on) and appropriately lighting the piece, a shadow profile of the lens was imaged onto a CCD camera and digitized. The radial position and sag depth information for the surface was measured using image processing software. A best fit functional form was then calculated from the data and compared with the intended design. Error bands were also calculated. Clearly, the fabricated lenses were not being manufactured to the original design specifications.

The focal spots for the other four lenses of the design were significantly poorer than that of lens 1. Moreover, the tube spacers that Plastec, Inc., manufactured did not match the lens diameters; however, their effort was cancelled before they could optimize the mechanical fit. At this point, it was concluded that Plastec, Inc., was not going to be able to meet the tight design specifications and an investigation was made to determine an alternative manufacturer of the lenslet elements.

Lenses from several alternative manufacturers were investigated including those from Precision Optics, Inc., and OPKOR, Inc. Commercially available glass aspheric lenses were purchased from Precision Optics, Inc., to assist in the evaluation of the optical design and lenslet testing procedure. Two of these lenses were set up as a simulation of the first two elements of a quad-asphere design. A large 3-bar target on the wall 57 inches away was imaged through a lenslet pair into a video camera. Figure 52a shows the 3-bar target as imaged directly by the camera without any intervening lenslets. The image obtained through the two lenslets, shown in Figure 52b, exhibited reduced contrast. The reduced contrast may be a result of the antireflection coatings on the lenslets. These lenslets were designed for use in conjunction with 0.8 μm laser diodes and not at the yellow wavelength where they were evaluated. The camera itself may also have contributed to the perceived loss of contrast due to a combination of electronic bandwidth in the digitizing and the size of the CCD pixels.

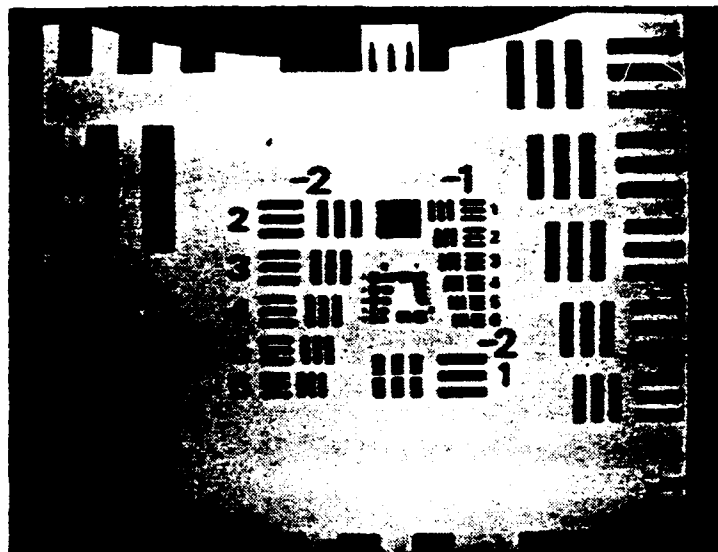


Figure 52a 3-Bar Test Chart as Seen Directly by Camera

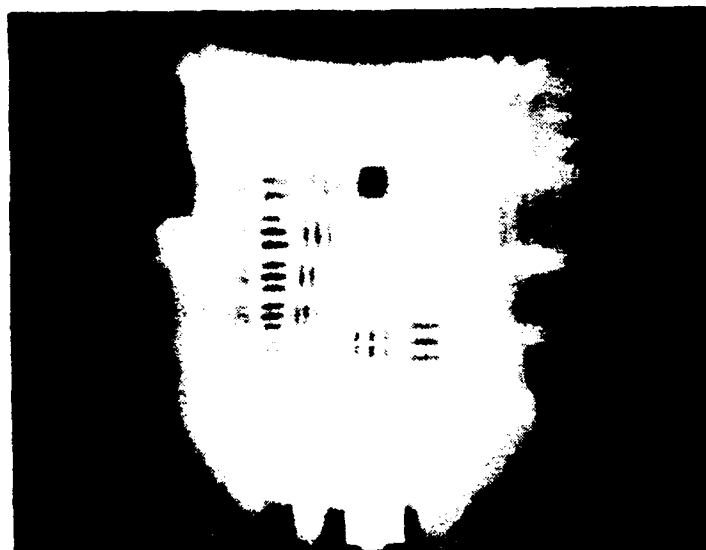


Figure 52b 3-Bar Test Chart as Seen by Two Precision Optics, Inc. Lenslets

Four of these lenses were mounted in a quad configuration. The performance of this quad was then evaluated using the 3-bar chart technique (Figure 53a). A 2.27 mm diameter aperture was used with a 50 mm focal length video lens. The contrast and image intensity were very low so frame averaging and contrast stretching were used to bring out the details and reduce the electronic noise.

Several plastic aspheric lenses were also received from OPKOR, Inc., for evaluation purposes. Four of these lenses were mounted in a quad configuration and evaluated with the 3-bar chart technique. The result of this evaluation is shown in Figure 53b. These lenses show slightly better performance than the Precision Optics lenses. This is probably due to the slightly higher quality lens surface and the fact that no antireflection coating is present on the OPKOR lenses.

The best lenses produced by Plastec, up to that point, were also evaluated by the 3-bar technique. Only two lenses were used in this imaging process due to the poor lens quality. Figure 53c shows the result of this experiment. As can be seen, significantly inferior results were obtained with these lenses as compared with either the Precision Optics or OPKOR lenses.

Finally, a fourth technique was developed to evaluate quantitatively the spot size near the focal region of the lenslets. Figures 54a through 54d show contour maps of the focal regions for the various lenslets evaluated. Figure 54a shows the spot size produced by a good quality 40x optical microscope objective lens. The microscope objective was used as a calibration device for this evaluation procedure. The circular contours in the center have the highest intensity and indicate a spot size of 2 μm . Figure 54b shows the results when a Plastec lenslet is evaluated. Here, very little circular symmetry is observed and the measured spot size is on the order of 50 μm . For comparison, both the Precision Optics and OPKOR lenslets were also evaluated. Both of these lenslets showed relatively good performance with spot sizes on the order of 3 μm . The Precision Optics lens is made of glass, is commercially available and is designed for use with semiconductor laser diodes. The OPKOR lens is 4 mm in diameter, made of plastic, and was custom molded for an unrelated project.

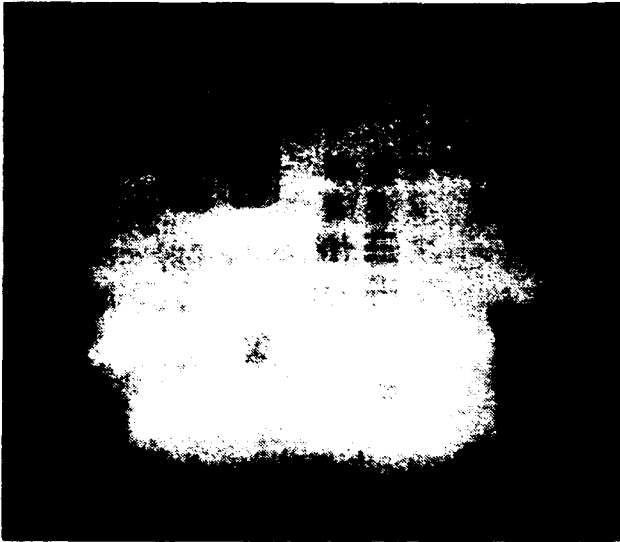


Figure 53a
3-Bar Test Chart as Viewed Through
Four Precision Optics, Inc. Lenslets
(This simulates a quad-lenslet unit.)

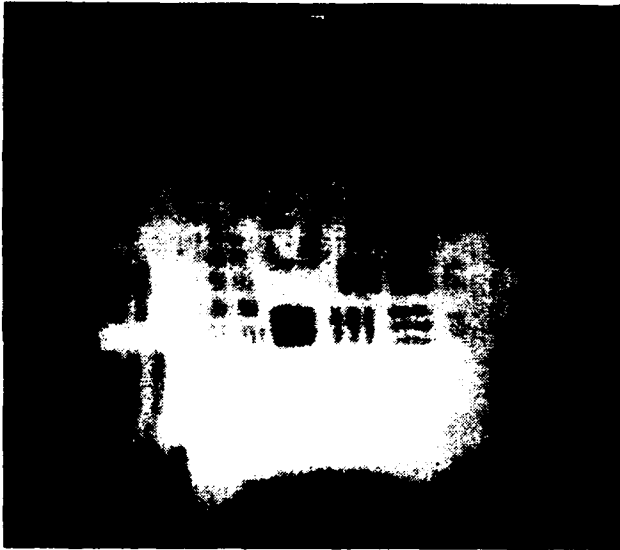


Figure 53b
3-Bar Test Chart as Viewed Through
Four OPKOR, Inc. Lenslets
(This simulates a quad-lenslet unit.)

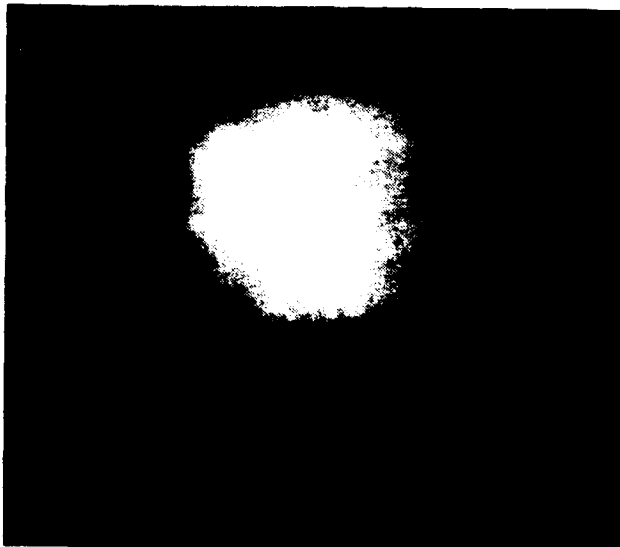
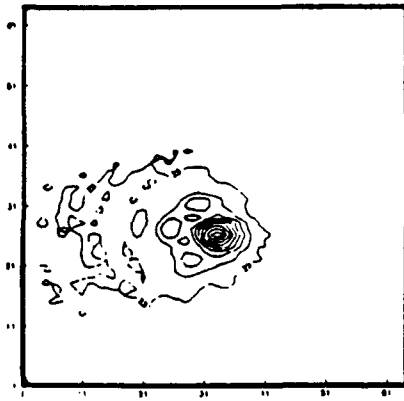
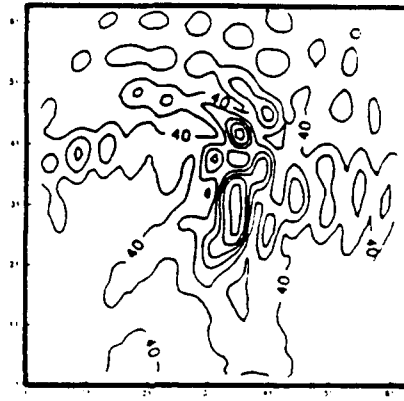


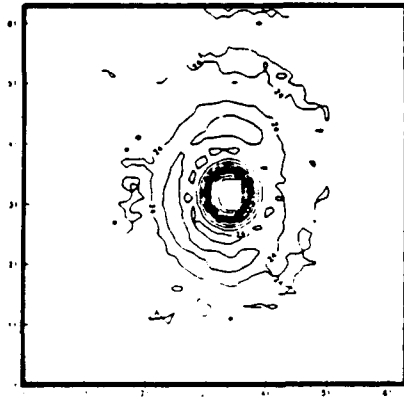
Figure 53c
3-Bar Test Chart as Viewed Through
Two Custom-Molded Plastec, Inc. Lenslets



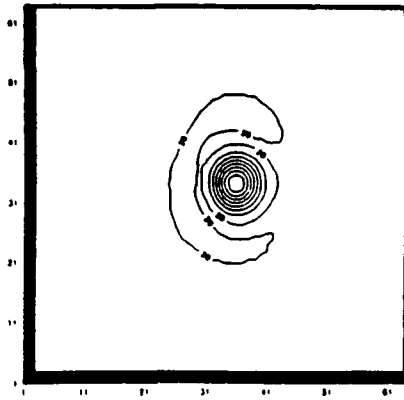
(a) Microscope Objective 40X



(b) Plastec, Inc.



(c) Commercial Lenslet



(d) OPKOR, Inc.

Figure 54 Focal Region Contour Maps for Various Lenslets Available

OPKOR, Inc., provided several lenslets to allow evaluation of their fabrication technology prior to our award of a subcontract to produce the custom molded lenslets. Based on an evaluation of their lenslets, a subcontract was initiated with OPKOR, Inc., to produce the first lens (lens 1) of the PROTO90Q design. Figure 54d shows diffraction limited performance for the OPKOR lenslet, significantly superior to the Plastec design of Figure 54b. On the basis of these results, it appeared that OPKOR, Inc., would be able to produce small, high quality optical lenslets. Figure 55 shows the results of this fabrication process for lens number one of the PROTO90Q design. Reproducible, diffraction-limited performance has been achieved by OPKOR, Inc., for the custom design.

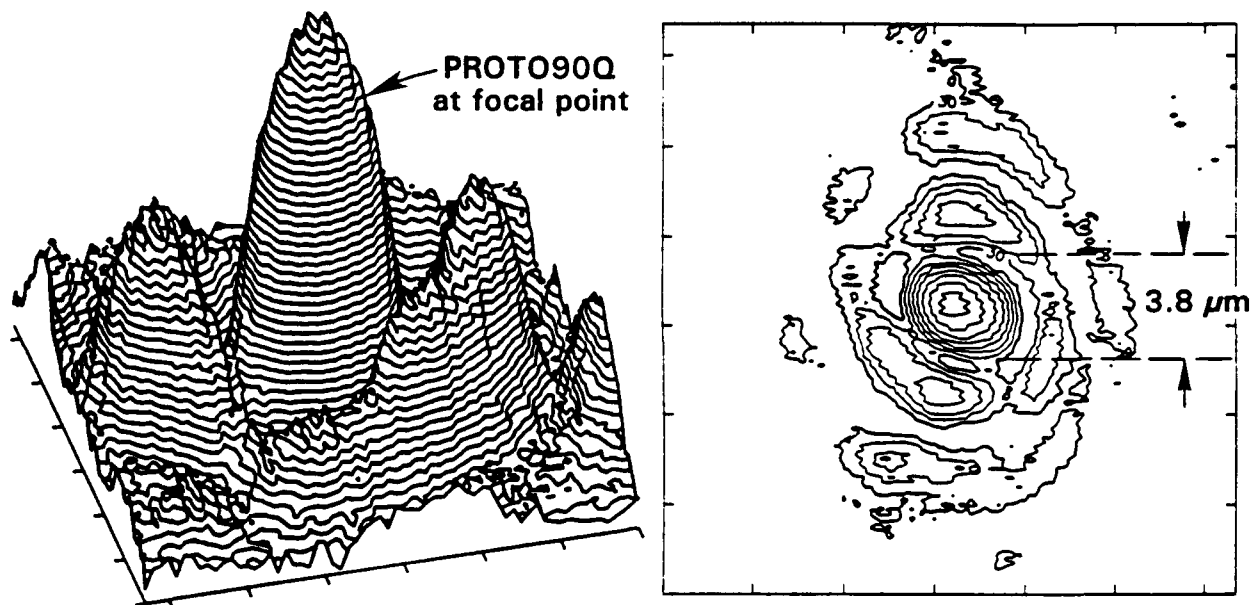


Figure 55 3-D Profile and Contour Map of Custom Molded Lens from OPKOR, Inc.

In order to assess the image quality produced by a theoretical system, a video image processing technique was developed using data from Super-Oslo and Matrox™ (an image processing system) utility codes. Super-Oslo provided spot size information as a function of position in the image plane. By convolving a real image with the theoretical spot size function, simulation of the image performance of any theoretical lens system was possible. An image of a tank was captured by the image processing system and placed on a high frequency grid background as shown in Figure 56. This was used as the reference during subsequent analysis. The tank image was then digitally processed using the theoretical PROTO90Q spot function information from Super-Oslo. This convolved image showed no degradation on-axis with only a blurring of the grid at the edge of the FOV. This is shown in Figure 57 and indicates the relative amount of degradation that might be seen by the human eye when looking through the PROTO90Q lenslet array. For experimental comparison, the tank and grid, imaged on a TV monitor, was photographed through four of OPKOR's evaluation

lenslets. The image of the tank as seen through the four lenslets is shown in Figure 58. These lenses were close in performance to the on-axis PROTO90Q design and showed good visual agreement between the real and processed images.

6.2 Estimated Manufacturing Costs

There are currently two basic ways to approach the manufacturing process. The first approach will be designated the "quad" approach and relies on making individual lenslets and spacers and then manually assembling them one-by-one and inserting them into some form of holder or eyepiece. This is the approach currently being pursued by Battelle. The second approach uses what is termed a monolithic approach, wherein all the lenses at a particular distance from the eye are molded at one time in a hemispherical configuration. Several hemispherical "shells" are then assembled and aligned to the accuracy required. As the design evolves, anywhere from four to about 8 or even 10 shells may be required. Obviously, the more shells, the more complicated the design and, hence, more expensive.

In discussions with OPKOR, Inc., each mold they make has a useful life of about 1,000,000 shots (molded plastic parts). Of this, their yield is about 90-92%. In production, they also have about a 10% down time for machine maintenance.

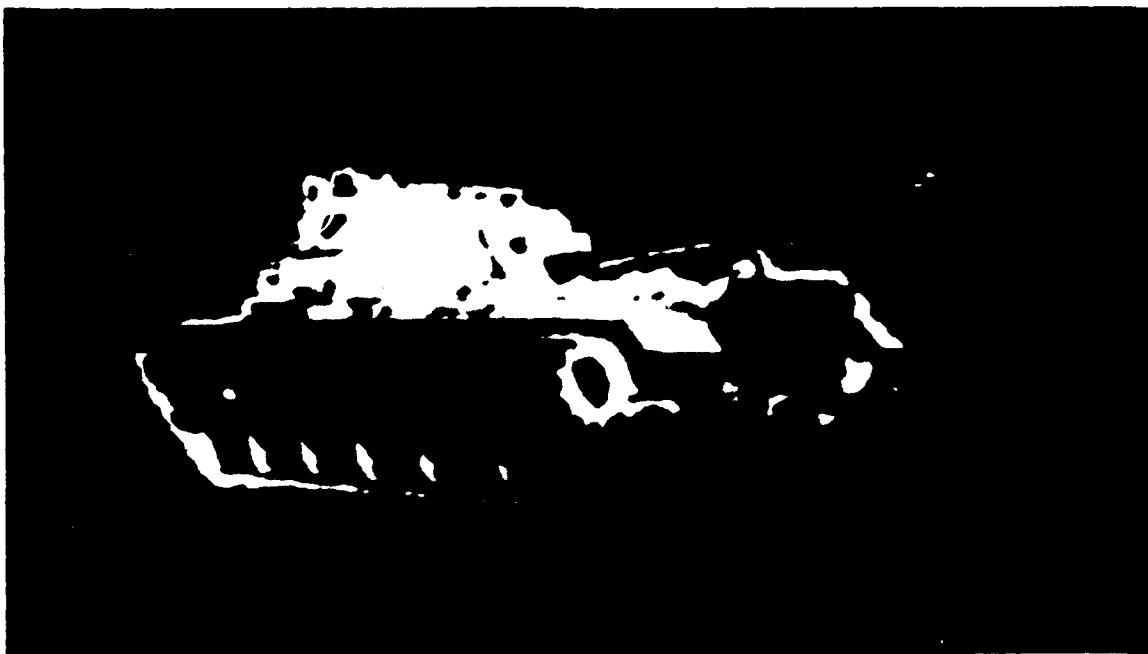


Figure 56 Photograph of Video Display High Contrast

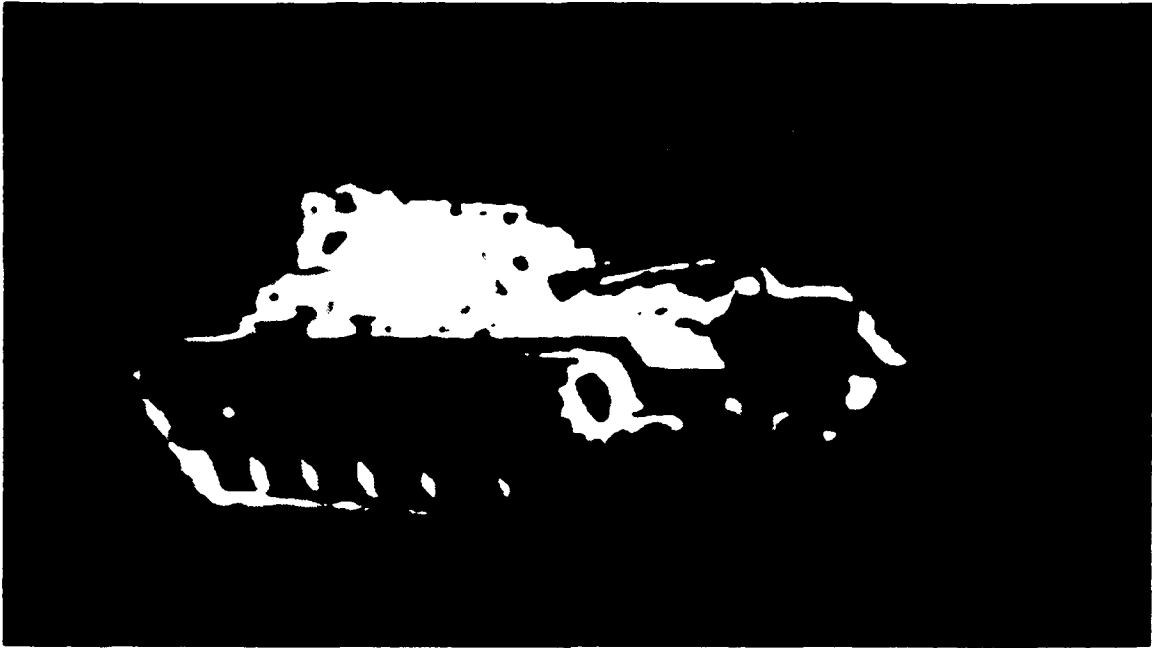


Figure 57 Computer Simulation Using PROTO90Q FOV Resolution

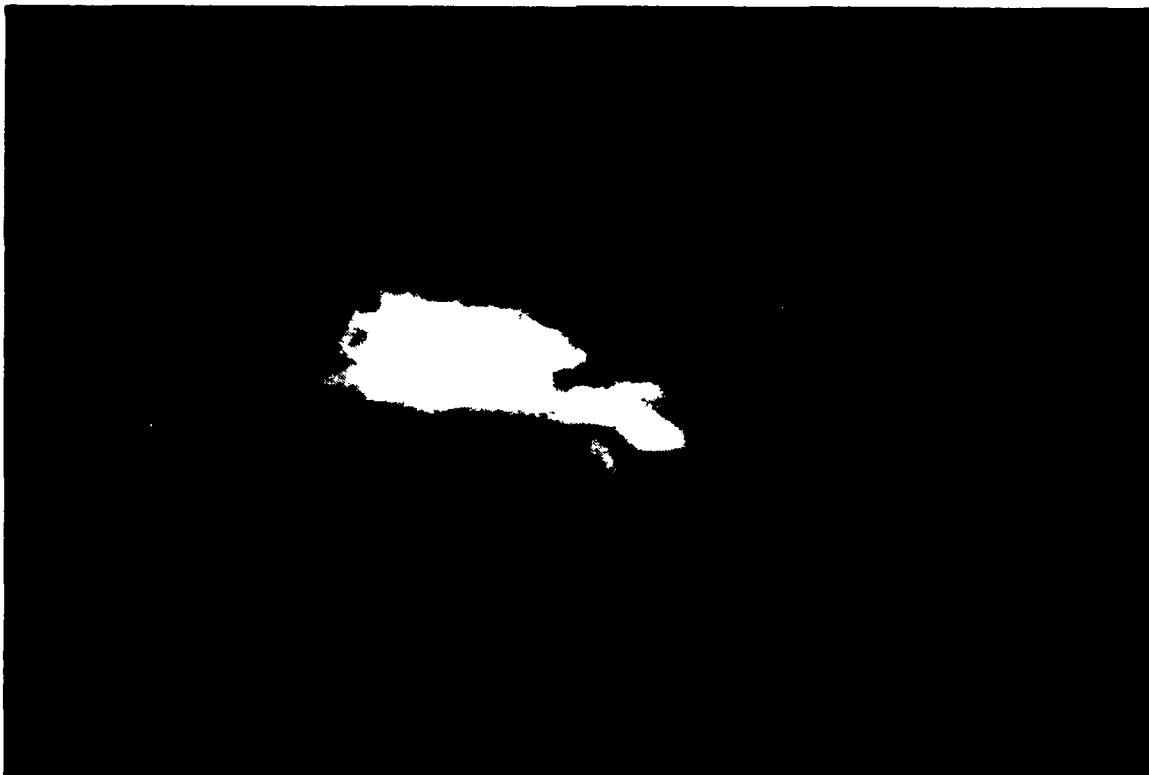


Figure 58 Photograph of Video Display Through OPKOR Quad

Consider now a quad manufacturing approach for the current design.

$$215 \text{ lenses/lens type/eye} * 2 \text{ eyes} * 70,000 \text{ units} = 30.1 \text{ M lenses/type}$$

$$30.1 \text{ M lenses/type} * 4 \text{ types} = 120.4 \text{ M lenses}$$

OPKOR's approach would be to make a 16 cavity tool for each type of lens. Each 16 cavity tool will produce 4-5 M lenses/year. Useful life of the 16 cavity tool is 16 M parts less 10%. The nonrecurring cost of a 16 cavity tool is estimated to be \$55-60 K. Volume production costs for each biaspheric lens would be \$0.15/lens.

Nonrecurring tooling costs to mount 1000 lenses so that they could be antireflection (AR) coated is estimated to be \$7-8000. High volume coating costs would be \$0.20/surface. This would be a multilayer coating resulting in 0.7% reflection loss/surface over the wavelength range 450-600 nm.

Nonrecurring costs to make the three spacers, as currently designed, is estimated at \$20-25 K. High volume production for spacers would be \$0.20/set of spacers.

Cementing the lenses into the spacers would be \$0.50/surface. The total of all these costs can be summarized in Table 2.

Table 2 Nonrecurring and Production Costs of Quads

Nonrecurring Costs		Production Costs	
Item	Cost	Item	Cost
Lens Cavities	\$240K	Four Lenses	\$ 0.60
Spacers	\$ 25K	Eight AR Coatings	\$ 1.60
Coating Adaptor	+ \$ 8K	Three Spacers	\$ 0.20
Tooling (Total)	\$273K	Cementing Six Surfaces	+ \$ 3.00
		Cost per Quad	\$ 5.40
		Quads/Goggles	x \$ 430.00
		Cost for Quads (Total)	\$2322.00

These costs do not include chromatic correction (possibly necessitating an additional lens), the nonlinear material and associated holder (possibly the cost of an additional lens for the holder plus NLO material costs), field lens, abrasion resistant coating on first and last lens, eyepiece cost (to hold the quad lens units), and goggle with straps to hold the eyepieces on the head. Finally there would be such additional costs as quality control and testing to ensure functionality.

The above analysis indicates a preliminary production cost of \$6.40/quad for a quad with the limitations as discussed above. Realistically this cost must be brought down to about \$1.00/quad for a goggle design that requires 430 quads. This would leave approximately \$500/goggle to address all the remaining deficiencies of this analysis. The two highest costs associated with the quad are the cementing/assembly costs and the AR coating costs. By increasing the number of lenses coated at one time from 1000 to 5000 the cost could be reduced from \$1.60/quad to \$0.32/quad. This results in a material cost of \$1.10/quad. The cementing costs are more difficult to assess and would appear to be a primary factor for abandoning this assembly technique in favor of the monolithic shell approach. Assuming a cementing/assembling cost of \$60/h and 6 surfaces/quad to be cemented, a \$3.00/quad cementing cost translates to 20 quads/h being assembled or 120 surfaces/h being cemented. This corresponds to about 30 s/surface. With automation this could possibly be reduced to about 5 s/surface, reducing the cementing cost to \$0.50/quad. This would bring the assembled quad cost to \$1.60/quad, or \$688.00 for the 430 quads necessary to populate the dome. Nonrecurring assembly automation costs could be several million dollars.

Extending the above assumptions to estimate the nonrecurring and production costs for a complete goggle device we have the following (Table 3).

Table 3 Nonrecurring and Production Costs of Goggles

Nonrecurring Costs		Production Costs	
Item	Cost	Item	Cost
Lens Cavities	4 x \$60K	Four Lenses	\$ 0.60
Chromatic Lens	1 x \$60K	Chromatic Lens	\$ 0.15
Field Lens	1 x \$60K	Field Lens	\$ 0.15
NLO Cavity	1 x \$60K	NLO Cavity	\$ 0.30
Spacers	\$ 50K	Spacers	\$ 0.20
Coating Adaptor	\$ 40K	AR Coatings	\$ 0.56
Eyepiece Cavity	\$ 200K	Cementing 12 Surfaces	+ \$ 6.00
Goggle Cavity	+ \$ 100K	Cost per Quad	\$ 7.96
Tooling Costs	\$ 810K	Quads/Goggle	x \$ 430.00
Quality Testing	+ \$1000K	Cost for Quads	\$3422.80
Total	\$1810K	Two Eyepieces	\$ 100.00
		Goggles	\$ 50.00
		Quality Testing	+ \$ 100.00
		Per Goggle Unit	\$3672.80

To produce the full number of units required would require one tool replacement due to the 30 M lenses of each type required and the finite lifetime of the tool of about 16 M. Assuming complete tool replacement we find total nonrecurring costs to be on the order of \$3,000,000 and per unit production costs of \$3700-4200/goggles.

By automating the assembly to 5 s/surface, the cementing costs can potentially be reduced from \$6.00/quad to \$1.00/quad, bringing the total quad cost to \$3.00/quad. 430 quads would then cost \$1290 and each completed goggle would cost \$1540.

Summarizing this approach, nonrecurring costs are on the order of \$5,000,000 and a per unit production cost of \$1500-2000/goggles. The production costs are about a factor of two greater than desirable.

Performing an optimistic cost evaluation, one can assume that kinoform optics can be used for the chromatic correction and, therefore, molded simultaneously as part of the other lenses. This would eliminate the need for a separate lens to correct chromatic aberrations. Also, we may assume that the field lens and the NLO holder can be combined in some manner as a single element.

This would eliminate the need for cementing three surfaces. Cost reductions for this assembly would then be \$0.15 for the chromatic lens, \$0.15 for the field lens, and \$0.25 for cementing. This reduces the cost of an assembled quad from \$3.00 to \$2.45. 430 quads would cost \$1053, and an entire device would cost \$1300. By making these minor fabrication changes, the production costs can be reduced by \$250 per goggle device. Combining the center two lenses into a single unit would also result in some cost saving. This analysis still assumes approximately \$5,000,000 in nonrecurring tooling costs. It is currently assumed that \$1300 per goggle device might be considered close to being reasonable.

Evaluation of the manufacturing costs for a monolithic device proceeds as follows. Currently, a two-cavity lenslet tool costs approximately \$15,000. Estimates for a 16-cavity tool are \$60,000. Crudely extrapolating these numbers for a 215-cavity tool results in approximately \$500,000. This would be the tooling costs for fabricating one shell of a monolithic device. Estimating that 5 to 6 shells will be required indicates a tooling cost of \$3,000,000. Also needed is the goggle tooling of \$100,000. By eliminating the quad approach, approximately \$2,000,000 is saved in designing an assembling/cementing machine. A testing machine with an estimated cost of \$1,000,000 is still required. Total nonrecurring costs for this approach would appear to be about \$4,000,000. Going to smaller-size lenses would increase the cost of the tooling; therefore, a safe, nonrecurring tooling cost might be \$5-10,000,000. If the production of each shell can be made for under \$50/each, an eyepiece consisting of 6 lenslet-populated shells would cost about \$300. In addition to this, we have the soft face mask for \$50/each. This results in a total cost of \$650/goggle device plus \$100 for quality control, which brings the total cost to \$750/unit. The required optical coatings have not been discussed for this approach but are estimated at about \$100. This would still keep the cost of each unit under \$1000. Note also that as one goes to smaller size lenses the idea of a quad assembly approach becomes totally nonviable and one is, therefore, forced into the monolithic approach.

7.0 CONCLUSIONS

During this program numerous lenslet elements were evaluated theoretically for their potential use in a self-activated eye protection device using nonlinear optics. This effort concentrated on assessing the feasibility of such an approach and included such issues as expected visual performance, resolution, field of view, mechanical tolerances, and nonlinear optical materials. The basic question to be resolved was whether or not you would be able to see through it.

At this point in the investigation, an aspheric lenslet design, referred to as PROTO90Q, has been developed, which theoretically provides near-diffraction-limited performance over a limited field of view. The design was initially to be fabricated by Plastec, Inc.; however, after repeated fabrication attempts Plastec, Inc., was unable to meet the stringent fabrication tolerances. Subsequently, an order was placed with OPKOR, Inc., to fabricate the first lens of the PROTO90Q design. The results of this fabrication effort were very successful. The optical quality of the lenslets received from OPKOR, Inc., was near diffraction-limited (theoretical best) and was of very high optical quality.

A hemispherical goggle concept was developed that appears to solve the field of view issue. The current design does not allow for motion of the eye, but this is believed resolvable. These lenslet eyepieces have been incorporated into the standard Army-issue sun, wind, and dust goggles for testing. Ultimately, custom goggles will have to be fabricated but these goggles currently provide a convenient mounting mechanism. In general, while the issue of design is a complex one, nothing has been found to preclude the use of lenslets as a viable goggle design; in fact, many of the initial issues concerning methodology, design development, and fabrication have become more clearly understood.

An optical lenslet design based completely on binary optics was also investigated during this program but was found to be unacceptable. An optical design was not found that even closely provides the optical image quality attainable with the currently chosen design. A substantial effort was made to evaluate various binary optical configurations, with limited success. The difficulty arises from the fact that binary optics is inherently monochromatic and to extend its performance over the visible region of the spectrum is extremely difficult. While a novel design may provide a viable solution to an all-binary optical approach, the prospects are highly unlikely. The use of binary optics seems to be most suited as a correction mechanism for refractive elements in this application.

As for the nonlinear optical material itself, only a preliminary assessment of this essential component has been performed. Our estimates indicate that current nonlinear optical materials have nonlinearities only one-tenth (optimistic) or one-hundredth (more realistic) of that required to achieve effective optical limiting depending on the particular optical design. A thorough

investigation has not been performed, however, and caution should be used when interpreting these observations. A specific design was not investigated, in terms of device functionality. These estimates were based upon the best nonlinear optical materials available and the best optical design with respect to optical gain. It is unlikely, however, that a device with such materials and design would have all the desired features in its first iteration.

In conclusion, Battelle believes it has a good understanding of the problem and understands many of the intricacies associated with the design. Battelle has resolved many of the questions associated with the design and fabrication of the device and has developed an approach to resolve the unresolved questions. Battelle is confident in their approach and methodology, but much work remains to develop a functional frequency-agile eye protection device.

8.0 RECOMMENDATIONS

It is proposed that this research be continued to optimize the designs established during this program and develop a second generation optical design with improved field of view, allow for motion of the eye, be chromatically corrected within limits, and incorporate currently available nonlinear optical material.

Further analysis is also required in understanding the effects on vision produced by the goggle device. The eye is a complex detector in that it has orbital motion as well as varying resolution dependent upon the angle of incident light. In addition, diffraction effects of the optical lenslet array must be considered. When an array is constructed with lenslet elements greater than 2 mm in diameter, the array of lenslets can add incoherently and still provide a reasonable degree of performance. However, when the array consists of microlenses with a diameter of less than 1 mm, the array must be designed to add coherently, producing a diffraction equivalent to the full aperture of the array, rather than of the individual elements, in order to have an acceptable level of performance.

Investigation of fabrication techniques should continue since they may affect greatly the overall optical performance of the device.

Modeling should also continue on nonlinear optical materials for use in the lenslet sandwich structure that would act to absorb, defocus, scatter, or otherwise disrupt the transmittance of laser threats while allowing lower intensity visible radiation to reach the eye for ordinary vision.

In summary, Battelle is committed to the development of a lenslet array suitable for eye protection against a frequency-agile visible laser source and recommends that, as the NLO materials develop, a global view of the problem be undertaken to integrate the NLO materials with the lenslet array device. Figure 59 shows a list of proposed future efforts, along with their timing, that are proposed to develop a completely functional eye protection device.

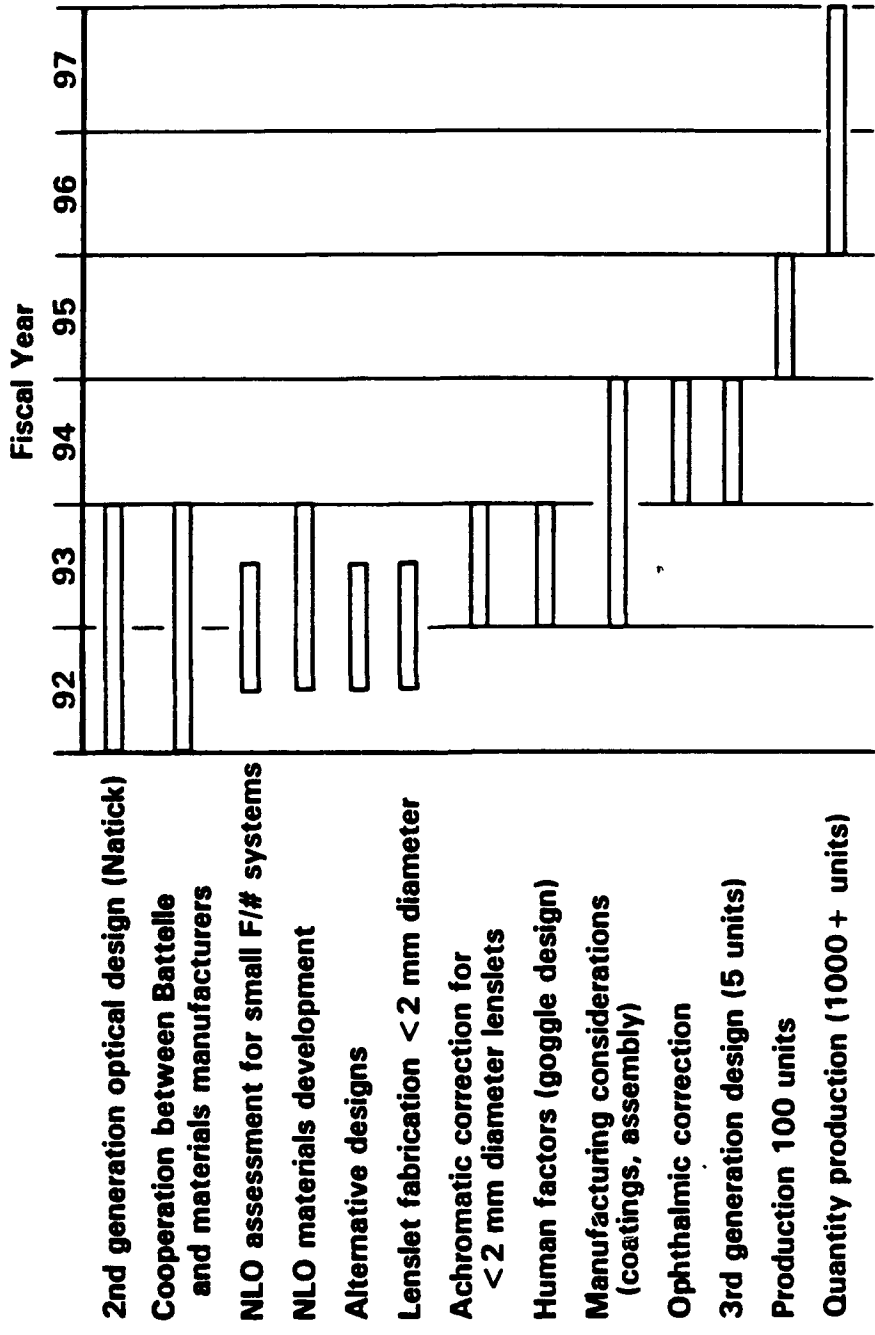


Figure 59 Proposed Future Efforts

9.0 REFERENCES

- (1) H. v. Helmholtz, Helmholtz's Treatise on Physiological Optics, Vol. 1, Translated from 3rd German edition, edited by J.P.C. Southall, Opt. Soc. of Amer., Rochester, New York (1924-1925).
- (2) F. W. Campbell and R. W. Gubisch, *J. Physiol. (London)* 186, 558 (1966).
- (3) M. Kato et al., *Appl. Opt.* 28, 682 (1989).
- (4) M. Alpern, *Arch. Ophthalmol.* 81, 518 (1969).
- (5) Y. R. Shen, *Prog. Quantum Electron.* 4, 1 (1975).
- (6) J. H. Marburger, *Prog. Quantum Electron.* 4, 35 (1975).
- (7) D. J. Hagan et al., *Proc. SPIE* 1105, 103 (1989).
- (8) E. W. Van Stryland et al., *J. Opt. Soc. Amer.* B5, 1980 (1988).
- (9) G. L. Wood et al., *Proc. SPIE* 1105, 154 (1989).
- (10) W. L. Smith, CRC Handbook of Laser Science and Technology, Vol. III, Part 1, 229 (CRC Press, 1986).
- (11) R. C. Hoffman et al., *J. Opt. Soc. Amer.* B6, 772 (1989).
- (12) J. A. Hermann, *Opt. and Quantum Electron.* 19, 169 (1987).